AD-A171 779 URBAN DISCRETE CLUTTER SOURCES(U) NEW HAMPSHIRE UNIV 1/1
DURHAM K SIVAPRASAD ET AL. JUL 86 SCEE-PDP-83-35
RADC-TR-86-70 F30602-81-C-0193

UNCLASSIFIED F/G 17/9 NL

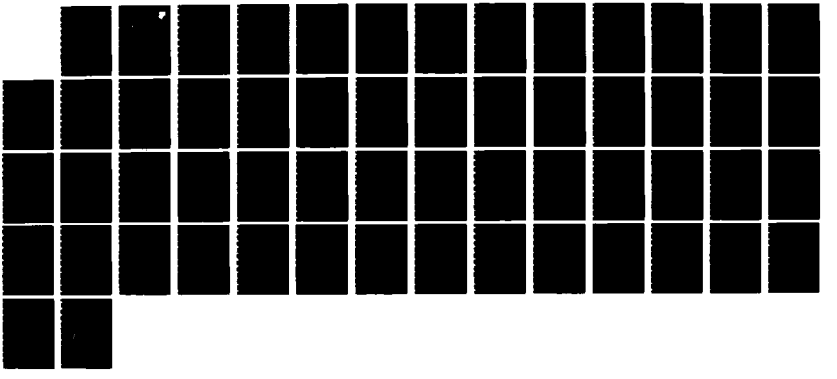

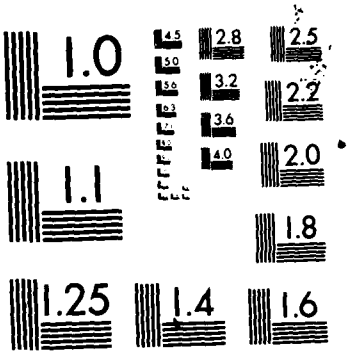

12

RADC-TR-86-70
Final Technical Report
July 1986

AD-A171 779

# URBAN DISCRETE CLUTTER SOURCES

University of New Hampshire

Kondagunta Sivaprasad
Allen Drake
Subramanyam D. Rajan



APPROVED FOR PUBLIC RELEASE; DISTRIBUTION UNLIMITED



ROME AIR DEVELOPMENT CENTER
Air Force Systems Command
Griffiss Air Force Base, NY 13441-5700

This report has been reviewed by the RADC Public Affairs Office (PA) and is releasable to the National Technical Information Service (NTIS). At NTIS it will be releasable to the general public, including foreign nations.

RADC-TR-86-70 has been reviewed and is approved for publication.

APPROVED: John F Lennon

JOHN F. LENNON
Project Engineer

APPROVED: Allan C Schell

ALLAN C. SCHELL
Chief, Electromagnetic Sciences Division

FOR THE COMMANDER: John A. Ritz

JOHN A. RITZ
Plans and Programs Division

If your address has changed or if you wish to be removed from the RADC mailing list, or if the addressee is no longer employed by your organization, please notify RADC (EECT) Hanscom AFB MA 01731-5000. This will assist us in maintaining a current mailing list.

Do not return copies of this report unless contractual obligations or notices on a specific document requires that it be returned.

AD-A171779

UNCLASSIFIED
SECURITY CLASSIFICATION OF THIS PAGE

# REPORT DOCUMENTATION PAGE

| | |
|---|---|
| 1a. REPORT SECURITY CLASSIFICATION<br>UNCLASSIFIED | 1b. RESTRICTIVE MARKINGS<br>N/A |
| 2a. SECURITY CLASSIFICATION AUTHORITY<br>N/A | 3. DISTRIBUTION/AVAILABILITY OF REPORT<br>Approved for public release; distribution unlimited |
| 2b. DECLASSIFICATION/DOWNGRADING SCHEDULE<br>N/A | |
| 4. PERFORMING ORGANIZATION REPORT NUMBER(S)<br>SCEE-PDP-83-35 | 5. MONITORING ORGANIZATION REPORT NUMBER(S)<br>RADC-TR-86-70 |
| 6a. NAME OF PERFORMING ORGANIZATION<br>University of New Hampshire<br>6b. OFFICE SYMBOL (If applicable) | 7a. NAME OF MONITORING ORGANIZATION<br>Rome Air Development Center (EECT) |
| 6c. ADDRESS (City, State, and ZIP Code)<br>Durham NH 03824 | 7b. ADDRESS (City, State, and ZIP Code)<br>Hanscom AFB MA 01731-5000 |
| 8a. NAME OF FUNDING/SPONSORING ORGANIZATION<br>Rome Air Development Center<br>8b. OFFICE SYMBOL (If applicable)<br>EECT | 9. PROCUREMENT INSTRUMENT IDENTIFICATION NUMBER<br>F30602-81-C-0193 |
| 8c. ADDRESS (City, State, and ZIP Code)<br>Hanscom AFB MA 01731-5000 | 10. SOURCE OF FUNDING NUMBERS<br>PROGRAM ELEMENT NO.: 61102F<br>PROJECT NO.: 2305<br>TASK NO.: J4<br>WORK UNIT ACCESSION NO.: P2 |

11. TITLE (Include Security Classification)
URBAN DISCRETE CLUTTER SOURCES

12. PERSONAL AUTHOR(S)
Kondagunta Sivaprasad, Allen Drake, Subramanyam D. Rajan

| 13a. TYPE OF REPORT | 13b. TIME COVERED | 14. DATE OF REPORT (Year, Month, Day) | 15. PAGE COUNT |
|---|---|---|---|
| Final | FROM Nov 84 TO Oct 85 | July 1986 | 58 |

16. SUPPLEMENTARY NOTATION
N/A

| 17. COSATI CODES | | | 18. SUBJECT TERMS (Continue on reverse if necessary and identify by block number) |
|---|---|---|---|
| FIELD | GROUP | SUB-GROUP | |
| 17 | 09 | | Scattering |
| 20 | 14 | | SAR Imagery |
| | | | Periodic Surfaces |

19. ABSTRACT (Continue on reverse if necessary and identify by block number)

A possible model for the urban areas viewed by SAR imagery is to consider them as a gridded periodic structure. Holford's integral equation method has been used to calculate the back-scattered intensity and the results indicate a variation in intensity as a function of aspect angle. This has been observed to be the case.

| | |
|---|---|
| 20. DISTRIBUTION/AVAILABILITY OF ABSTRACT<br>☐ UNCLASSIFIED/UNLIMITED ☒ SAME AS RPT. ☐ DTIC USERS | 21. ABSTRACT SECURITY CLASSIFICATION<br>UNCLASSIFIED |
| 22a. NAME OF RESPONSIBLE INDIVIDUAL<br>John F. Lennon | 22b. TELEPHONE (Include Area Code)<br>(617) 861-3735<br>22c. OFFICE SYMBOL<br>RADC (EECT) |

DD FORM 1473, 84 MAR 83 APR edition may be used until exhausted. All other editions are obsolete.

SECURITY CLASSIFICATION OF THIS PAGE
UNCLASSIFIED

Table of Contents

List of Figures

## I. Introduction

The synthetic aperture radar on SeaSat Satellite has provided high resolution synoptic images of the earth's surface. However, the same geographical regions viewed at different look angles sometimes provided different images. This especially was the case of the images in the urban areas surrounding the Los Angeles areas (1). In these images the areas of the bright returns did not correspond while certain areas of low backscatter were common to both the images. A study of the causes of this variation in the imagery is the subject matter of the present report.

A possible model for the study of backscatter from urban areas due to the synthetic aperture radar is to consider it as a periodic gridded structure with the streets and the buildings forming the grid. The average dimensions of the grid for our study must have dimensions large compared to the wavelength.

As part of this task a literature survey was conducted and the principal relevant references were found to be due to DeSanto (2), Jordan & Lang (2), Holford (4), Uretsky (5), and McCammon and McDaniel (7). Uretsky's method which is based on the Helmholtz equation reduces the scattering from a periodic surface to an infinite set of linear equations of the form [A] [X] = [Y]. DeSanto also arrived at the same result using a different approach. For solving the infinite set of equations, the method of reduction was employed. In the method of reduction a truncation of the infinite series is employed and the correctness of the solution will depend on the order of matrix. However, for equations of the first kind, there does not exist, at present, a criteria for truncation which will assure the convergence of the solution.

Holford's method, like that of Uretsky, is based on the Helmholtz integral formula and results in a Fredholm integral equation of the second kind for the scattered intensity. This reduces his integral equation to the form

$$\left|\underline{[I]} + \underline{[A]}\right| [X] = [Y]$$

and rigorous proof exists for the convergence of the solutions. We, therefore, plan to use the approach due to Holford to study the scattering from a periodic surface. The only numerical results available using Holford's approach is due to McCammon and McDaniel and here they consider only relatively shallow structures, viz, for $Kh \sim 1$, where h is the height of the structure, $K = 2\pi/\Lambda$ and $\Lambda$ is the periodicity.

Section II of the report contains a detailed review of the relevant literature. Section III has the results of the backscatter calculations for a typical geometry suited for our observations using the exact method due to Holford. Section IV has the conclusions and the recommendations for future work on the problem.

---


1. SeaSat Views of North America, The Caribbean, and Western Europe with Imaging Radar, JPL Publication, 60-67, California Institute of Technology, Pasadena, CA.
2. J.A. DeSanto (1981), Rad. Sci. 16 p. 1315.
3. A.K. Jordan and R.A. Lang (1979), NRL Report 8284.
4. R.L. Holford (1981) JASA 70 p. 1116.
5. J.L. Uretsky (1966), Ann. Phys. 33 p. 400.
6. D.F. McCammon and S.T. McDaniel (1985), JASA 78 p. 149.

## II. Review of the Literature

The general methods of treating periodic structures can be broadly classified into two general approaches. The first approach are the so-called approximate methods and the second are the more exact methods. Sections II-1 and II-2 review briefly the approximate methods, while Sections II-3 through II-5 review the more exact methods. In Section II-6, some of the details, that have to be considered, for the numerical implementation of the calculations for the Holford's method are discussed.

### II-1 Kirchoff Method

The general Kirchoff Method is based on Helmholtz integral equation. Consider a plane wave incident on a rough surface. The scattered field at any observation point P is

$$E_2(P) = \frac{1}{4\pi} \iint (E \frac{\partial \psi}{\partial n} - \psi \frac{\partial E}{\partial n}) \, ds \tag{1}$$

where the integral is over the surface and E is the field on the surface. $\psi$ is the free space Green's function $(\exp(ikR')/R')$,

$$\psi = \frac{e^{ikR'}}{R'} \tag{2}$$

where R' is the distance from the origin to P and $k = (2\pi/\lambda)$. In the above equation, E is an unknown. The Kirchoff approximation assumes

$$E = (1 + R)E_1 \text{ and } (\frac{\partial E}{\partial n})_s = (1 - R)E_1(\bar{k} \cdot \bar{n}) \tag{3}$$

where $\bar{n}$ is the normal to this surface at P and R is the reflection coefficient of a smooth plane. In the case of an one dimensional surface where $L = \zeta(x)$, and R = +1, Beckman (1963) arrives at the following for the scattering coefficient, $\rho$

A Beckmann and A. Spizzichino (1963). "The Scattering of Electromagnetic Waves from Rough Surfaces", Pergammon Press.

$$\rho\ (\theta_1,\theta_2) = (E_2/E_0) = \sec\theta_1 \left[\frac{1+\cos(\theta_1+\theta_2)}{\cos\theta_1+\cos\theta_2}\right] \cdot \frac{1}{\Lambda}\int_{-\Lambda/2}^{\Lambda/2} e^{i\bar{r}\cdot\bar{v}}dx \qquad (4)$$

$\theta_1$ is the direction of the incident field, $E_2$ is the field reflected in the direction $\theta_2$ and

$$\bar{r}\cdot\bar{v} = \frac{2\pi}{\lambda}\left[(\sin\theta_1 - \sin\theta_2)x - (\cos\theta_1 + \cos\theta_2)\zeta(x)\right] \qquad (5)$$

This approximation is valid when $\Lambda >> \lambda$ and the radius of curvature of the irregularities is large compared to the wave length. Consequently, this method will break down when there are sharp edges.

II-2 Rayleigh Method

In the Rayleigh Method, the field is expressed as a sum of plane waves whose directions correspond to the scattering angles and for a periodic surface, the scattering direction will be given by the grating equation. So for a periodic surface $\zeta(x)$

$$\zeta(x) = h\cos Kx \qquad (6)$$

The grating equation for the field is

$$\sin\theta_{2m} = \sin\theta_0 + mK/k \qquad m = 0, \pm1, \pm2,\ldots \qquad (7)$$

The total field in the region $z>\zeta(x)$, E, (eq. 8), is the sum of the incident field, $E_1$, and the reflected field, $E_2$,

$$\begin{aligned} E &= E_1 + E_2 \\ &= e^{iR_1\cdot\bar{r}} + \sum_{m=-\infty}^{\infty} A_m e^{iR_{2m}\cdot\bar{r}} \end{aligned} \qquad (8)$$

where

$$R_{2m} = k(\hat{e}_x \sin\theta_{2m} + \hat{e}_z \cos\theta_{2m})$$

$$K_1 = k(\hat{e}_x \sin\theta_0 - \hat{e}_z \cos\theta_0)$$

$$\bar{r} = (x\hat{e}_x + y\hat{e}_y + z\hat{e}_z)$$

and $\hat{e}_x$, $\hat{e}_y$ and $\hat{e}_z$ are the unit vectors in the x,y and z direction. For the case of the Dirichlet boundary, $E|_{z=\zeta(x)} = 0$. So, from Equations (7) and (8), we have

$$e^{-ik\zeta(x)\cos\theta_0} = -\sum_{m=-\infty}^{\infty} A_m e^{+imkx + ik\zeta(x)\cos\theta_{2m}} \tag{9}$$

Expanding both sides of Equation (9) in terms of Bessel functions, Beckman et al. (1963) arrives at the expression for the coefficient $A_m$

$$J_n(kh\cos\theta_0) = \sum_{m=-\infty}^{\infty} (-i)^m A_m J_{n+m}(kh\cos\theta_{2m}) \tag{10}$$

From this set of equations, the coefficients $A_m$ are determined, which are used in Equation 8 to obtain the field.

Uretsky (1966) notes that the major error in the solution given in Equation 8 is its implication that it describes the field everywhere above the surface. This has also been pointed out by Lipman (1953) that the solution does not take into account both up and down going waves excited in the "valley" of periodic surface. We will now describe two methods of solving the problem, both based on the integral equation formulation, starting from the Helmholtz equation, which will take into account both the upgoing and downgoing waves in the periodic structure.

---

B.A. Lipman (1953), J. of Op. Soc. Am., 43.

II-3 Uretsky's Method

This section describes the method proposed by Uretsky (1966) for solving the boundary value problem. For simplicity we consider a two dimensional problem and the scalar wave equation. The problem reduces to the solution of the two dimensional equation

$$\left[\frac{\partial^2 P(x,z)}{\partial x^2} + \frac{\partial^2 P(x,z)}{\partial z^2} + k^2\psi\right] = 0 \tag{11}$$

subject to boundary conditions which can be either soft, i.e., $P(x,z) = 0$ on the boundary, or hard, i.e., $\frac{\partial P(x,z)}{\partial n} = 0$, or an impedence boundary condition, i.e. $\frac{\partial P}{\partial n} + AP = 0$ on $\zeta(x)$, where A is a constant. Specifically, we will consider a surface

$$z = \zeta(x) = h\cos Kx \quad \text{where } K = (2\pi/\Lambda) \tag{12}$$

The field is now the sum of the incident field $P_{inc}(x,z)$ and the scattered field, P, given by the Helmholtz integral.

$$P(x,z) = P_{inc}(x,z) + \frac{1}{4i}\int_B P(r')\left[\frac{\partial H_o^{(1)}(k|\bar{r}-\bar{r}'|)}{\partial n'}\right.$$

$$\left. -H_o^{(1)}(k|\bar{r}-\bar{r}'|)\ \frac{\partial P(r')}{\partial n'}\right]ds \tag{13}$$

where $r' = (x', \zeta(x'))$ and the integral is taken along the boundary. In the case of a soft boundary, $(P(r') = 0)$

$$P(r) = P_{inc}(r) + \frac{k}{4}\int_{-\infty}^{\infty} \psi(x')\ H_o^{(1)}(k|\bar{r}-\bar{r}'|)\ dx' \tag{14}$$

where

$$\psi(x) = \left(\frac{i}{k}\frac{\partial P}{\partial n}\frac{ds}{dx}\right)_{z=\zeta(x)}$$

$$= \frac{i}{k}\left(-\frac{\partial P}{\partial z} + \zeta'(x)\ \frac{\partial P}{\partial x}\right)_{z=\zeta(x)} \tag{15}$$

As Equation 11 is unaffected by a shift of $2\pi/\Lambda$ and the boundary condition is also unaffected because it has a periodicity equal to $2\pi/\Lambda$, we can make the following expansion for $\psi(x)$.

$$\psi(x) = \sum_{n=-\infty}^{\infty} \psi_n e^{ik\alpha_n x} \tag{16}$$

where

$$\begin{aligned} \sin\theta_n &= \alpha_n = (\alpha_o + n\ K/k) \\ \cos\theta_n &= \gamma_n = (1-\alpha_n^2)^{1/2};\ \alpha_n \leq 1 \\ &= i(-1+\alpha_n^2)^{1/2};\ \alpha_n > 1 \end{aligned} \tag{17}$$

Substitution of the above in Equation (14) yields (Holford (1981))

$$P(r) = P_{inc}(r) + \sum_{n=-\infty}^{\infty} \psi_n \sum_{m=-\infty}^{\infty} e^{ik\alpha_m x}\ I_{m,n}(z) \tag{18}$$

where

$$I_{m,n}(z) = \frac{1}{2\pi i} \int_{-\infty}^{\infty} C_{m-n}(k\tau)\ \frac{e^{ik\tau z}\, d\tau}{\tau^2 - \gamma_m^2} \tag{19}$$

$$C_n(t) = \frac{1}{\Lambda} \int_0^{\Lambda} e^{-it\zeta(x) - inKx}\, dx \tag{20}$$

Holford (1981) has shown that the integral $I_{m,n}(z)$ is given by

$$I_{m,n}(z) = \frac{1}{2\gamma_m} C_{m-n}(k\gamma_m) e^{ik\gamma_m z} \qquad z > \zeta(x) \tag{21}$$

Also the field $P(x,z)$ can be written as

$$P(x,z) = P_{inc}(x,z) + \sum_{n=-\infty}^{\infty} R_n e^{ik\alpha_n x + ik\gamma_n z} \tag{22}$$

Inserting Equation 21 into Equation 18 and comparing with Equation 22, we obtain

$$R_m = \frac{1}{2\gamma_m} \sum_{n=-\infty}^{\infty} \psi_n\ C_{m-n}(k\gamma_m) \tag{23}$$

We now proceed to determine the $\psi_n$. In the Equation (18), we let the field

point, r approach the boundary.

$$P(r)\Big|_{z=\zeta(x)} = P_{inc}(r)\Big|_{z=\zeta(x)} + \frac{k}{4}\int_{-\infty}^{\infty} \psi(x')\, H_0^{(1)}(k|r-r'|)dx' \tag{24}$$

If we now apply the boundary condition that $P(r) = 0$ we have

$$\frac{k}{4}\int_{-\infty}^{\infty} \psi(x')\, H_0^{(1)}\,(k|r-r'|)dx' = -\,P_{inc}(x) \tag{25}$$

Substituting Equation (16) in Equation (25)

$$\frac{k}{4}\int_{-\infty}^{\infty} \left(\sum_n \psi_n e^{ik\alpha_n x'}\right) H_0^{(1)}\,(k\mu)dx' = -P_{inc}(x) \tag{26}$$

where $\mu = [(x-x')^2 + (\zeta(x) - \zeta(x'))^2]^{1/2}$

Applying the operator

$$\frac{1}{\Lambda}\int_0^{\Lambda} e^{-ik\alpha_m x}dx \tag{27}$$

to both sides of Equation (26), we obtain on substituting, $P_{inc}(x,z) = e^{ik\alpha_0 x - ik\gamma_0 z}$, from Eq. 8.

$$\sum_{n=-\infty}^{\infty} \psi_n\, V_{m,n} = -2C_m(k\gamma_0)\quad m = 0, \pm1, \pm2, \ldots \tag{28}$$

where $V_{m,n}$

$$= \frac{1}{\Lambda}\int_0^{\Lambda} e^{-ik\alpha_m x}dx \int_{-\infty}^{\infty} \frac{k}{2} H_0^{(1)}\,(k\mu)e^{+ik\alpha_n x'}\,dx' \tag{29}$$

This set of linear equations (Equation 28) is used to solve for $\psi_n$ which is then substituted in (Equation 23) to obtain $R_n$.

Note that the set of linear equations is of the form $AX = Y$. The procedure recommended by Uretsky (1966) is to truncate the set at some value $n=N$ and then solve the linear equation by matrix inversion. However as Holford (1981) has pointed out there is no guarantee that the solution for $AX = Y$ will converge as

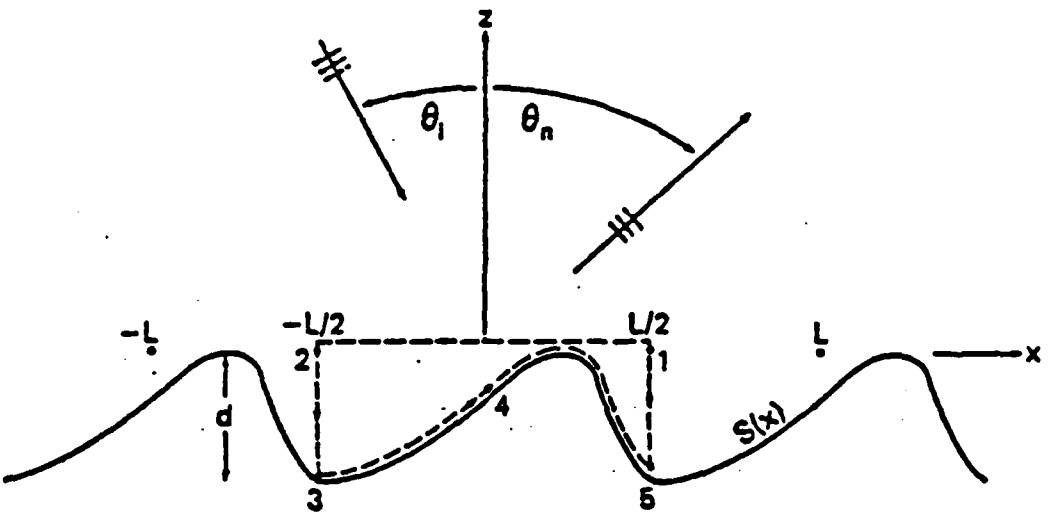


Fig. 1. Plane wave scattering from a surface $s(x)$ of period $L$ and depth $d$. The closed contour (123451) is used for Green's theorem. The incidence angle is $\theta_i$, and $\theta_n$ is one of the discrete scattering angles. Diagram lines are slightly offset for clarity.

$m \to \infty$ or will converge to a correct solution. This method is valid only for equations of the second kind represented by $(I + A)X = Y$ where I is an identity operator. Holford's method of overcoming this will be discussed later in Section II-5.

## II-4 Method of Desanto

Desanto (1981) has proposed another approach which is similar to that of Uretsky. For a sinusoidal surface shown in Figure 1 and a plane wave incident on the surface.

$$\psi_i(x,z) = e^{ik\alpha_0 x - ik\gamma_0 z} \tag{30}$$

where

$\theta_0$ = incident angle

$\alpha_0 = \sin\theta_0$,

$\gamma_0 = \cos\theta_0$

The reflected field is then

$$\psi_r(x,z) = \sum_n A_n e^{ik\alpha_n x + ik\gamma_n z} \tag{31}$$

where

$$\sin\theta_n = \alpha_n = \alpha_0 + n\,\lambda/\Lambda = \alpha_0 + n\,K/k \quad n = 0, \pm 1, \pm 2, \ldots$$

$$\cos\theta_n = \gamma_n$$

The Green's function

$$G^{\pm}(x,z) = (e^{\pm(ik_0\gamma_m z - ik_0\alpha_m x)}) \tag{32}$$

satisfies the wave equation in the region $z>0$. We now consider the contour 12345 in Figure 1 and apply the Green's theorem to the contour

$$\int_c (\psi \frac{\partial G^{\pm}}{\partial n} - G^{\pm} \frac{\partial \psi}{\partial n}) d_\mu = 0 \tag{33}$$

and

$$\psi(x,z) = \psi_{inc}(x,z) + \sum_{n=-\infty}^{\infty} A_n e^{ik_o\alpha_n x + ik\gamma_n z} \tag{34}$$

If we now let 23 and 51 shrink to zero, then the integral along the path 12 becomes

$$I_{12} = \int_{-\Lambda/2}^{+\Lambda/2} \{\pm ik_o\gamma_m e^{ik_o(\alpha_o-\alpha_m)x} \pm ik_o\gamma_m \sum_n A_n e^{ik_o(\alpha_n-\alpha_m)} + ik_o\gamma_o e^{ik_o(\alpha_o\mp\alpha_m)x} - ik_o\sum_n A_n\gamma_n e^{ik_o(\alpha_n\mp\alpha_m)x}\}\, dx \tag{35}$$

For $G^+$ along 1-2, Eq. 35 reduces to

$$I_{12} = -4\pi i\gamma_m(\Lambda/\lambda)\delta_{mo} \tag{36}$$

and for $G^-$ along 1-2, Eq. 35 simplifies to

$$I_{12} = (4\pi i\gamma_m \frac{\Lambda}{\lambda}) A_m \tag{37}$$

Hence

$$I_{12} = (4\pi i\gamma_m \frac{\Lambda}{\lambda}) \begin{cases} -\delta_{mo} & \text{for } G^+ \\ A_m & \text{for } G^- \end{cases} \tag{38}$$

The integral along 23 and 51 are zero since we have allowed 2 to approach 3 and 5 to approach 1. The equation simplifies to

$$\int_{12} (\psi \frac{\partial G^+}{\partial n} - G^+ \frac{\partial \psi}{\partial n})\, d\mu + \int_{345} (\psi \frac{\partial G^+}{\partial n} - G^+ \frac{\partial \psi}{\partial n})\, d\mu = 0 \tag{39}$$

or

$$\int_{345} (\psi \frac{\partial G^+}{\partial n} - G^+ \frac{\partial \psi}{\partial n})\, d\mu = -\int_{12} (\psi \frac{\partial G^+}{\partial n} - G^+ \frac{\partial \psi}{\partial n})\, d\mu \tag{40}$$

$$= (4\pi i\gamma_m \frac{\Lambda}{\lambda_o}) \begin{cases} \delta_{mo} & \text{for } + \\ -A_m & \text{for } - \end{cases}$$

We now need to evaluate the left hand side of the equation. Let us assume Dirichlet boundary condition.

$$-\int_{345} (G^{\pm} \frac{\partial \psi}{\partial n})\, d\mu = -(4\pi i \gamma_m \frac{\Lambda}{\lambda_o}) \begin{cases} -\delta_{mo} & \text{for } + \\ A_m & \text{for } - \end{cases} \tag{41}$$

Following the method of Uretsky, we now replace $\frac{\partial}{\partial n} \psi(x,\zeta(x))d\mu$ by $\phi(x)dx$, where $\phi(x)$ is a periodic function with a period $\Lambda$.

$$\phi(x) = \frac{2\pi}{\Lambda} e^{ik_o \alpha_o x} B(x) \tag{42}$$

where $$B(x) = 2 \exp[-ik_o d\gamma_o(1 + \cos(2\pi/\Lambda)x)] \sum_{n=-\infty}^{\infty} i^n a_n \exp(in2\pi x/\Lambda). \tag{42a}$$

Substituting Eq. 42 to the right hand side of Eq. 41, we obtain

$$\int_{345} G^{\pm}(x,\zeta(x)) \frac{\partial \psi}{\partial n}\, d\mu$$

$$= \int_{-\Lambda/2}^{\Lambda/2} G^{\pm}(x,\zeta(x)) \frac{2\pi}{\Lambda} e^{ik_o \alpha_o x} B(x)dx \tag{43}$$

Now, let $\zeta(x) = -\frac{d}{2}(1 + \cos\frac{2\pi x}{\Lambda})$ and let $y = \frac{2\pi}{\Lambda} x$,

$$\int_{345} G^{\pm}(x,\zeta(x)) \frac{\partial \psi}{\partial n}\, d\mu$$

$$= -e^{\mp(ix_o d\gamma_m/2)} \int_{-\pi}^{\pi} e^{\mp(ik_o d\gamma_m \cos y/2 - imy)} C(y)dy \tag{44}$$

where

$$C(y) = B(\frac{\Lambda}{2\pi} y)$$

Using equation 41, we obtain for $G^+$

$$\int_{-\pi}^{\pi} C(y) e^{(-imy - ik_o d\gamma_m \cos y/2)} = \frac{\Lambda 4\pi i \gamma_m}{\lambda_o} e^{(ik_o d/2\gamma_m)} \delta_{mo} \tag{45}$$

and for $G^-$

$$\int_{-\pi}^{\pi} C(y) \exp[-imy + i(k_o d\gamma_m \cos y/2)]\, dy = -A_m(4\pi i\gamma_o/\lambda_o) \exp(-ik_o d\gamma_m/2) \tag{46}$$

From Eqs. 44(a) and (42a)

$$C(y) = -\left(\frac{2i\gamma_o\Lambda}{\lambda_o}\right)e^{(ik_o d\gamma_o(1+\cos y)/2)}\ \{1 + \sum_{n\neq o} i^n a_n e^{iny}\} \tag{47}$$

Substituting for C(y) from Equation 47 in Equation (45), then yields the set of linear equations for $m\neq 0$

$$J_m(\tau_m^-) + \sum_{n\neq o} a_n\, J_{m-n}(\tau_m^-) = 0 \tag{48}$$

Similarly, substitution in Equation (46) gives

$$A_m = -\left(\frac{\gamma_o}{\gamma_m}\right) i^m \exp(i\tau_m^+)\ \{J_m(\tau_m^+) + \sum_{n\neq o} a_n\, J_{m-n}(\tau_m^+)\} \tag{49}$$

where

$$\tau_m^{\pm} = (\gamma_o \pm \gamma_m)\,\frac{k_o d}{2}$$

We, therefore, solve the first set of linear equations to obtain $a_n$ which is then used in Equation 49 to obtain the $A_m$.

Jordan and Lang (1979) solved the Equations 48 and 49 numerically. They state that no numerical instability was experienced and the stability of the method was checked by testing conservation of energy (i.e) $\sum_n |R_n|^2 \frac{\gamma_n}{\gamma_o} = 1$ for real orders of n. Wirgin (1980) reports that the method of Desanto was also used by Whitman and Schwering (1977) who reported no instability for $Kh \leq 1$ and $Kh \leq 2.36$. However, in their experience this method does not work well for $Kh > \pi$. Further Wirgin states that the solution will become unstable for $Kh \geq \pi$.

A. Wirgin, (1980), JASA 68, p. 692.

G. Whitman and S. Schwering, (1977), IEEE. PGAP 25, p. 869.

Though Jordan and Lang reported no instability in their numerical computation, as the equations are of the form AX = Y, convergence to the correct solution cannot be guaranteed..

## II-5 Method Due to Holford

Holford (1981) has developed a method to overcome this problem. This method is similar to the approach of Uretsky, where we start with the two dimensional boundary value problem and seek a solution to the differential equation satisfying the given boundary conditions on the surface and the radiative condition at $x^2 + z^2 \to \infty$.

### II-5-1: Surface Satisfying the Dirichlet Boundary Condition:

Applying the Helmholtz integral formula as in Section II-3 we obtain for the Dirichlet boundary condition,

$$P(r) = P_{inc}(r) + \frac{k}{4} \int_{-\infty}^{\infty} \psi(x') H_0^{(1)}(k|\bar{r}-\bar{r}'|)\, dx' \tag{50}$$

where

$$\psi(x) = \left(\frac{i}{k} \frac{\partial P}{\partial n} \frac{ds}{dx'}\right)_{z=\zeta(x)} \tag{51}$$

Let the normal derivative operator $ik^{-1}[-\frac{\partial}{\partial z} + \zeta'(x) \frac{\partial}{\partial x}]$ be applied to both sides and taking on the limit when $z \to \zeta(x)$, we obtain

$$\psi(x) = \hat{\psi}(x) + \frac{k}{4} \int_{-\infty}^{\infty} \psi(x') \left[-\frac{\partial}{\partial z} + \zeta'(x) \frac{\partial}{\partial x}\right] H_0^{(1)}(k|\bar{r}-\bar{r}'|)dx' \tag{52}$$

It has been shown by Meecham (1956) that the integrand on the right hand side has a singularity at $\bar{r} = \bar{r}'$ and this integrates to a term $\frac{1}{2}\psi(x)$ in the limit.

---

W.C. Meecham (1956), J. Rat. Mech. Analysis 5 p. 323.

Thus, we have

$$\frac{1}{2}\psi(x) = \hat{\psi}(x) - \frac{ik}{4}\int_{-\infty}^{\infty}\psi(x')\frac{H_1^{(1)}(k|\bar{r}-\bar{r}'|)}{|\bar{r}-\bar{r}'|} \tag{53}$$

$$\cdot [(\zeta(x') - \zeta(x)) - (x'-x)\zeta'(x)]dx$$

where

$$\hat{\psi}(x)=(+ik^{-1})\cdot[-\frac{\partial}{\partial z} + \zeta'(x)\frac{\partial}{\partial x}]e^{ik\alpha_o x - ik\gamma_o z}$$

$$= -[\gamma_o + \alpha_o\zeta'(x)]e^{ik\alpha_o x - ik\gamma_o\zeta(x)} \tag{54}$$

We therefore obtain

$$\psi(x) + \frac{ik}{2}\int_{-\infty}^{\infty}\psi(x')\frac{H_1^{(1)}(k|\bar{r}-\bar{r}'|)}{|\bar{r}-\bar{r}'|}[(\zeta(x') - \zeta(x)) - \zeta(x'-x)\zeta'(x)]dx'$$

$$= 2\hat{\psi}(x) \tag{55}$$

As explained in Section II-III, $\psi(x)$ is periodic with the period $\Lambda$. So

$$\psi(x) = \sum_{n=-\infty}^{\infty}\psi_n e^{ik\alpha_n x} = \sum_{n=-\infty}^{\infty}\psi_n e^{ik(\alpha_o+nK/k)x}$$

$$= e^{ik\alpha_o x}\sum_n\psi_n e^{inKx} \tag{56}$$

Substituting for $\psi(x)$ in the above expression

$$\sum_n\psi_n e^{ik\alpha_n x} + \frac{ik}{2}\sum_n\psi_n\int_{-\infty}^{\infty} e^{ik\,n\,x'}(H_1^{(1)}(k|\bar{r}-\bar{r}'|)/|r-r'|)$$

$$[(\zeta(x') - \zeta(x)) - (x'-x)\zeta'(x)]dx' = 2\hat{\psi}(x) \tag{57}$$

We now apply the operator

$$\frac{1}{\Lambda}\int_0^{\Lambda} e^{-ik\alpha_m x}\,dx \tag{58}$$

to both sides of the equation and obtain

$$\psi_m + \sum_n \psi_n U_{m,n} = 2\hat{\psi}_m \tag{59}$$

where

$$U_{m,n} = \frac{1}{\Lambda}\int_0^{\Lambda} e^{-ik\alpha_m x}\,dx\,\frac{k}{2}\int_{-\infty}^{\infty} e^{ik\alpha_n x'}\,\frac{H_1^{(1)}(k|\bar{r}-\bar{r}'|)}{|\bar{r}-\bar{r}'|}$$

$$[(\zeta(x') - \zeta(x)) - (x'-x)\zeta'(x)]dx' \tag{60}$$

and

$$\hat{\psi}_m = \frac{1}{\Lambda}\int_0^{\Lambda}\hat{\psi}(x)e^{-ik\alpha_m x}\,dx$$

$$= -\frac{1}{\Lambda}\int_0^{\Lambda}(\gamma_0 + \alpha_0\zeta'(x))e^{ik\alpha_0 x} - ik\gamma_0\zeta(x)\,dx \tag{61}$$

This set of linear equations (Eq. 59) is now solved to determine $\psi_n$ and then $\psi(x)$. This is then used to obtain $P(\bar{r})$. The specular reflection coefficients for various orders of scattering is obtained from Equation (23) which is reproduced below

$$R_m = \frac{1}{2\gamma_m}\sum_{n=-\infty}^{\infty}\psi_n\, C_{m-n}(k\gamma_m) \tag{62}$$

II-5-2: Surface Satisfying the Neumann Boundary Condition:

Applying the boundary condition $\frac{\partial p}{\partial n} = 0$, in Eq. 13, we obtain

$$P(r) = P_{inc}(r) + \frac{1}{4i}\int_{-\infty}^{\infty}\phi(x')\,\frac{\partial}{\partial n'}[H_0^{(1)}(k|\bar{r}-\bar{r}'|)]_{(z'=\zeta(x'))}\,\frac{ds'}{dx'}\,dx' \tag{63}$$

where $\phi(x') = P(x',\zeta(x'))$. We now let $r \to [x,\zeta(x)]$, then using the same method as was used in deriving Eq. 52, we obtain

$$\frac{1}{2}\phi(x) = \hat{\phi}(x) + \frac{ik}{4}\int_{-\infty}^{\infty}\phi(x')\frac{H_1^{(1)}(k|\bar{r}-\bar{r}'|)}{|r-r'|}$$

$$[(\zeta(x) - \zeta(x')) - (x-x')\zeta'(x')]\,dx' \tag{64}$$

$$\phi(x) = 2\hat{\phi}(x) + \frac{ik}{2}\int_{-\infty}^{\infty}\phi(x')\frac{H_1^{(1)}(k\mu)}{\mu}C(x,x')\,dx' \tag{64a}$$

where

$$C(x,x') = [(\zeta(x) - \zeta(x')) - (x-x')\zeta'(x')] \tag{65}$$

$$\mu = [x-x')^2 + (x(x)-x(x'))^2]^{1/2}$$

where $\hat{\phi}(x) = P_{inc}(x, \zeta(x))$. We now write

$$\phi(x) = \sum_{n=-\infty}^{\infty}\phi_n e^{ik\alpha_n x} \tag{66}$$

Substituting in equation (64a), we obtain

$$\sum_n \phi_n e^{ik\alpha_n x} - \int_{-\infty}^{\infty} C(x,x')\left(\sum_n \phi_n e^{ik\alpha_n x'}\right)\frac{ik}{2}\frac{H_1^{(1)}(k\mu)}{\mu}dx' = 2\hat{\phi}(x) \tag{67}$$

Applying the operator $\frac{1}{\Lambda}\int_0^{\Lambda} e^{-ik\alpha_m x}dx$ to both sides, we obtain

$$\phi_n - \frac{1}{\Lambda}\int_0^{\Lambda} e^{-ik\alpha_m x}dx \int_{-\infty}^{\infty}\left(\sum_n \phi_n e^{ik\alpha_n x'}\right)\frac{ik}{2}\left[\frac{H_1^{(1)}(k\mu)}{\mu}\right]C(x,x')\,dx'$$

$$= 2\,\frac{1}{\Lambda}\int_0^{\Lambda}\hat{\phi}(x)e^{-ik\alpha_m x}\,dx \tag{68}$$

$$\phi_m - \sum_n \phi_n U_{m,n} = \hat{\phi}_m \tag{69}$$

where $U_{m,n}$ is given by

$$U_{m,n} = \frac{1}{\Lambda}\int_0^{\Lambda} e^{-ik\alpha_m x}\,dx \int_{-\infty}^{\infty}\frac{ik}{2}\frac{H_1^{(1)}(k\mu)}{\mu}e^{-ik\alpha_n x'}C(x,x')\,dx' \tag{70}$$

The set of linear equations obtained can now be solved to yield $\phi_n$ which then can be substituted in the Equation 63 to yield P(r). The reflection coefficient for this case is given by the following expression (Holford).

$$R_m = \frac{1}{2\gamma_m} \sum_n \phi_n \, C_{m-n}(K\gamma_m)\left(\gamma_m + \frac{(m-n)K\alpha_m}{k\gamma_m}\right) \tag{71}$$

We note that in this case, the equation for $\phi_n$ is in form $(I + A)X = Y$ and therefore, convergence is guaranteed.

## II-6 Numerical Implementation of Holford Method

We will now describe the numerical implementation of the method due to Holford, as we will be discussing the results in the following Section III. Specifically we will consider the case where the surface is a sinusoidal surface and satisfies Neumann conditions. We, therefore, have

$$\zeta(x) = h \cos Kx$$

The linear set of equations to be solved is

$$\phi_m - \sum_n \phi_n V_{m,n} = \hat{\phi}_m \qquad m = 0, \pm 1, \ldots \tag{72}$$

where $V_{m,n}$ is given by

$$V_{m,n} = \frac{1}{\Lambda} \int_0^{\Lambda} dx \, e^{-ik\alpha_m x} \frac{ik}{2} \int_{-\infty}^{\infty} e^{ik\alpha_n x'} \frac{H_1^{(1)}(k|\bar{r}-\bar{r}'|)}{|\bar{r}-\bar{r}'|} \Big|_{z = \zeta(x)}$$

$$(\zeta(x) - \zeta(x') - (x - x')\zeta'(x')) \, dx' \tag{73}$$

Where

$$|\bar{r}-\bar{r}'| = [(x - x')^2 + (\zeta(x) - \zeta'(x'))^2]^{1/2} \tag{74}$$

Let $\tau = (x-x')$

$$V_{m,n} = \frac{1}{\Lambda} \int_0^{\Lambda} e^{-ik\alpha_m x} dx \int_{-\infty}^{\infty} e^{ik\alpha_n x'} \, K(\tau, x') dx' \tag{75}$$

where

$$K(\tau,x') = \frac{ikh}{2}\frac{H_1^{(1)}(k\rho)}{\rho}\left((\cos Kx - \cos Kx') + K\tau \sin Kx'\right) \tag{76}$$

and

$$\rho = [\tau^2 + h^2(\cos Kx - \cos Kx')^2]^{1/2} \quad .$$

Then,

$$V_{m,n} = \frac{1}{\Lambda}\int_0^{\Lambda} e^{ik\alpha_n x'}\,dx' \int_{-\infty}^{\infty} e^{-ik\alpha_m x}\,K(\tau,x')dx$$

$$= \frac{1}{\Lambda}\int_0^{\Lambda} e^{-ik(\alpha_m-\alpha_n)x'}dx' \int_{-\infty}^{\infty} e^{-ik\alpha_m x}\,e^{+ik\alpha_m x'}\,K(\tau,x')dx'$$

$$= \frac{1}{\Lambda}\int_0^{\Lambda} e^{-i(m-n)Kx'}dx' \int_{-\infty}^{\infty} e^{-ik\alpha_m \tau}K(\tau,x')d\tau \tag{77}$$

where $k(\alpha_m-\alpha_n) = K(m-n)$

and $K(\tau,x')$ is given by Equation (75). To determine $V_{m,n}$, we consider $V_{m,n}$ as

$$V_{m,n} = \hat{V}_{m,n} + (V_{m,n} - \hat{V}_{m,n}) \tag{78}$$

where $\hat{V}_{m,n}$ is obtained using $\hat{K}(\tau, x')$ in the Equation (74) $\hat{K}(\tau,x')$ is different fro $K(\tau,x')$ in that $\rho$ is set equal to $\tau$. (i.e) the cosine terms in $\rho$ are neglected. This manipulation will simplify the final computation of $V_{m,n}$.

$$\hat{V}_{m,n} = \frac{1}{\Lambda}\int_0^{\Lambda} e^{-i(m-n)Kx'}dx' \int_{-\infty}^{\infty} e^{-ik\alpha_m \tau}\hat{K}(\tau,x')d\tau \quad .$$

$$= \frac{1}{\Lambda}\int_0^{\Lambda} e^{-iaKx'}x' \int_{-\infty}^{\infty} e^{-ib\tau}\hat{K}(\tau,x')d\tau$$

$$= \frac{1}{\Lambda}\int_{-\infty}^{\infty} e^{ib\tau}d_\tau \int_0^{\Lambda} e^{-iaKx'}\hat{K}(\tau,x')dx' \tag{79}$$

$$\hat{K}(\tau,x') = \frac{ik}{2}\frac{H_1^{(1)}(k|\tau|)}{|\tau|}[\zeta(x'+\tau) - \zeta(x') - \tau\zeta'(x')] \tag{80}$$

where $a = (m-n)$ and $b = -k\alpha_m$

Integrating with respect to $x'$,

$$\hat{V}_{m,n} = \frac{1}{\Lambda}\int_{-\infty}^{\infty} e^{ib\tau}d\tau \int_0^{\Lambda} \frac{ik}{2}\frac{H_1^{(1)}(k|\tau|)}{|\tau|}[\zeta(x'+\tau) - \zeta(x') - \tau\zeta'(x')]\, e^{-iaKx'}\, dx' \tag{81}$$

Let

$$\zeta_a = \frac{1}{\Lambda}\int_0^{\Lambda}\zeta(x')e^{-iaKx'}dx' \ . \tag{82}$$

Then from the periodicity of the terms in the integrand, we have

$$\hat{V}_{m,n} = \frac{ik}{2}\int_{-\infty}^{\infty} e^{-ib\tau}\frac{H_1^{(1)}(k|\tau|)}{|\tau|}[\zeta_a(e^{iaK\tau}-1-iaK\tau)]\, d\tau \tag{83}$$

This integral is in the form of Weber-Schasheitlin type (Watson 1944) and it gives

$$\hat{V}_{m,n} = i\zeta_a\left[\frac{aKb}{(k^2-b^2)^{1/2}} + \sqrt{k^2 - (b + aK)^2} - \sqrt{k^2-b^2}\right] \tag{84}$$

Substituting for a and b, we have

$$\hat{V}_{m,n} = i\zeta_{m-n}\left[\frac{(n-m)K\alpha_m}{\gamma_m} - k\gamma_m + k\gamma_n\right] \tag{85}$$

In the case of a pure sinusoid, of the form hcosKx, the fourier coefficients are $h/2$ for $a = \pm 1$.

$$\hat{V}_{m,n} = i\frac{h}{2}\left[\frac{(n-m)K\zeta_m}{\gamma_m} + k(\gamma_n-\gamma_m)\right] \qquad |m-n| = 1$$

$$= 0 \qquad |m-n| \neq 1 \tag{86}$$

G.N. Watson. A Treatise on Bessel Functions, Cambridge Univ. Press Cambridge, England, 1944.

The next step is to evaluate $(V_{m,n} - \hat{V}_{m,n}) = V^d_{m,n}$.

$$V^d_{m,n} = \frac{1}{\Lambda}\int_0^{\Lambda} e^{-ik\alpha_m x}\, dx \int_{-\infty}^{\infty} e^{+ik\alpha_n x'} f(x,x')\, dx' \tag{87}$$

$$f(x,x') = ik\left[-\frac{H_1^{(1)}(k\rho)}{2\rho} - \frac{H_1^{(1)}(k\hat{\rho})}{2\hat{\rho}}\right)\left((\zeta(x) - \zeta(x')) - (x-x')\zeta'(x')\right)dx'$$

$$\rho = \left[(x-x')^2 + (\zeta(x) - \zeta(x'))^2\right]^{1/2} \tag{88}$$

$$\hat{\rho} = (x-x')$$

writing the integral over the infinite limits as a sum

$$V^d_{m,n} = \frac{1}{\Lambda}\int_0^{\Lambda} e^{-ik\alpha_m x}\, dx \sum_{q=-\infty}^{\infty} \int_0^{\Lambda} e^{ik\alpha_n x'} f(x,x' + q\Lambda)\, dx'$$

$$= \frac{1}{\Lambda}\int_0^{\Lambda} e^{-ik\alpha_m x}\, dx \int_0^{\Lambda} e^{ik\alpha_n x'} \left(\sum_{q=-\infty}^{\infty} f(x,x' + q\Lambda)\, dx'\right) \tag{89}$$

$$= \frac{1}{\Lambda}\int_0^{\Lambda} e^{-ik\alpha_o x - imkx}\, dx \int_0^{\Lambda} e^{ik\alpha_o x' + iknx'} \left(\sum_{q=-\infty}^{\infty} f(x,x' + qn)\, dx'\right.$$

$$= \frac{1}{\Lambda}\int_0^{\Lambda} e^{-imkx}\, dx \int_0^{\Lambda} e^{iknx'} \hat{f}(x,x')dx'$$

where

$$\hat{f}(x,x') = e^{-ik\alpha_o(x-x')} \sum_q f(x,x' + q\Lambda). \tag{90}$$

We can easily evaluate $\hat{f}(x,x')$ and determine its fourier coefficients corresponding to m and n. We will show that, as the point $x \to x'$ and $q = 0$, $\hat{f}(x,x')$ is bounded. To show this, we take a sinusoidal surface represented by $\zeta(x) = h\cos Kx$

$$f(x,x') = \left(\frac{H_1^{(1)}(k\rho)}{\rho} - \frac{H_1^{(1)}(k\hat{\rho})}{\hat{\rho}}\right)\left[(h\cos Kx - h\cos Kx') + h(x-x')K\sin Kx'\right] \tag{91}$$

writing $x = x' + \tau$ as before

$$f(x,x') = \left(\frac{H_1^{(1)}(k\rho)}{\rho} - \frac{H_1^{(1)}(k\hat{\rho})}{\hat{\rho}}\right)[h\cos K(x'+\tau) - h\cos Kx' + hK\tau\sin Kx'] \quad (92)$$

as $x \to x'$, $\tau \to 0$

$$h[\cos(Kx'+K\tau) - \cos Kx' + K\tau\sin Kx']$$

$$= h[\cos Kx'\cdot\cos K\tau - \sin Kx'\sin K\tau - \cos Kx' + K\tau\sin Kx'] \quad (93)$$

For small values of $\tau$, $\sin K\tau = K\tau$ and $\cos K\tau = \left(1 - \frac{K^2\tau^2}{2}\right)$. Therefore, the right-hand side of Equation 93 now becomes $[-\cos Kx'(hK^2\tau^2/2)]$. By a similar argument, we write for small values of $\tau$

$$\rho = \tau(1 + h^2K^2\sin^2 Kx')^{1/2} \quad (94)$$

Also for small argument

$$H_1^{(1)}(z) \sim -\frac{1}{\pi i}\left(\frac{2}{z}\right) \quad (95)$$

Substituting all these in the expression for $f(x,x')$ we obtain

$$\underset{\substack{x\to x'\\ q\to 0}}{f(x,x')} = \frac{h^3K^4\cos Kx'\sin^2 Kx'}{i\pi k(1 + h^2K^2\sin^2 Kx')} \quad (96)$$

$f(x,x')$ can therefore be evaluated without difficulty and a 2D FFT is performed to obtain the elements of the matrix $V^d_{m,n}$.

From Equation 71, we have

$$[I - \hat{\nabla} - \nabla^d]\bar{\psi} = 2\bar{\hat{\psi}} \quad (97)$$

The expression for $\hat{V}_{m,n}$ has a singularity at $\gamma_m = 0$ and therefore we multiply each equation by the corresponding $\gamma_m$

$$[\bar{\gamma} - \bar{\gamma}\hat{\nabla} - \bar{\gamma}\nabla^d]\bar{\psi} = 2\bar{\gamma}\bar{\hat{\psi}} \quad (98)$$

where $\bar{\gamma}$ is a diagonal matrix containing $\gamma_m$ along the diagonal.

The method of Holford can also be used to calculate the scattering strength due to a beam of finite bandwidth by the following scheme.

The incident plane wave is split into its fourier components given by

$$B(\alpha_o) = \frac{1}{2\pi} \int_{-\infty}^{\infty} P_{inc}(x,k) e^{-ik\alpha_o n} dx \tag{99}$$

The resultant scattered field is computed from

$$P_{scat}(x,z) = \int_{-\infty}^{\infty} B(\alpha_o)\, \hat{P}_{scat}(x,z;\alpha_o)\, d\alpha_o \tag{100}$$

where $\hat{P}_{scat}(x,z,\alpha_o)$ is the scatter field due to unit amplitude plane wave incident upon the surface with a direction cosine $\alpha_o$.

## III. Results

A possible model for study of the urban areas with a SAR would be to model the surface as a rectangular periodic surface with a period of 30m and a height of about 15m. For an incident wave length of above .235m, the number of scattering angles will be of the order of 300 and a corresponding 300 x 300 matrix for obtaining the scattering intensities at these angles. Because of such a large matrix inversion, a smaller period for the surface was picked. It is felt that this scaled down model will also exhibit the principal characteristics of the original model we are interested in. The computation involves estimating the scatter intensities at discrete angles given by the grating equation using the exact method due to Holford. This was done at different incident angles ranging from 5° to 25°, with the corresponding back scatter directions given by -5° to -25° respectively. Higher angles were not considered as bulk of the energy was scattered in the forward direction at these angles. Also the look angles for SAR is in the region $20° \pm 3°$.

The issues in the numerical implementation of the scheme are

(a) The infinite sum in Equation (2.89) can be approximated by a finite number of terms and a length of $10\Lambda$ was sufficient to obtain con-

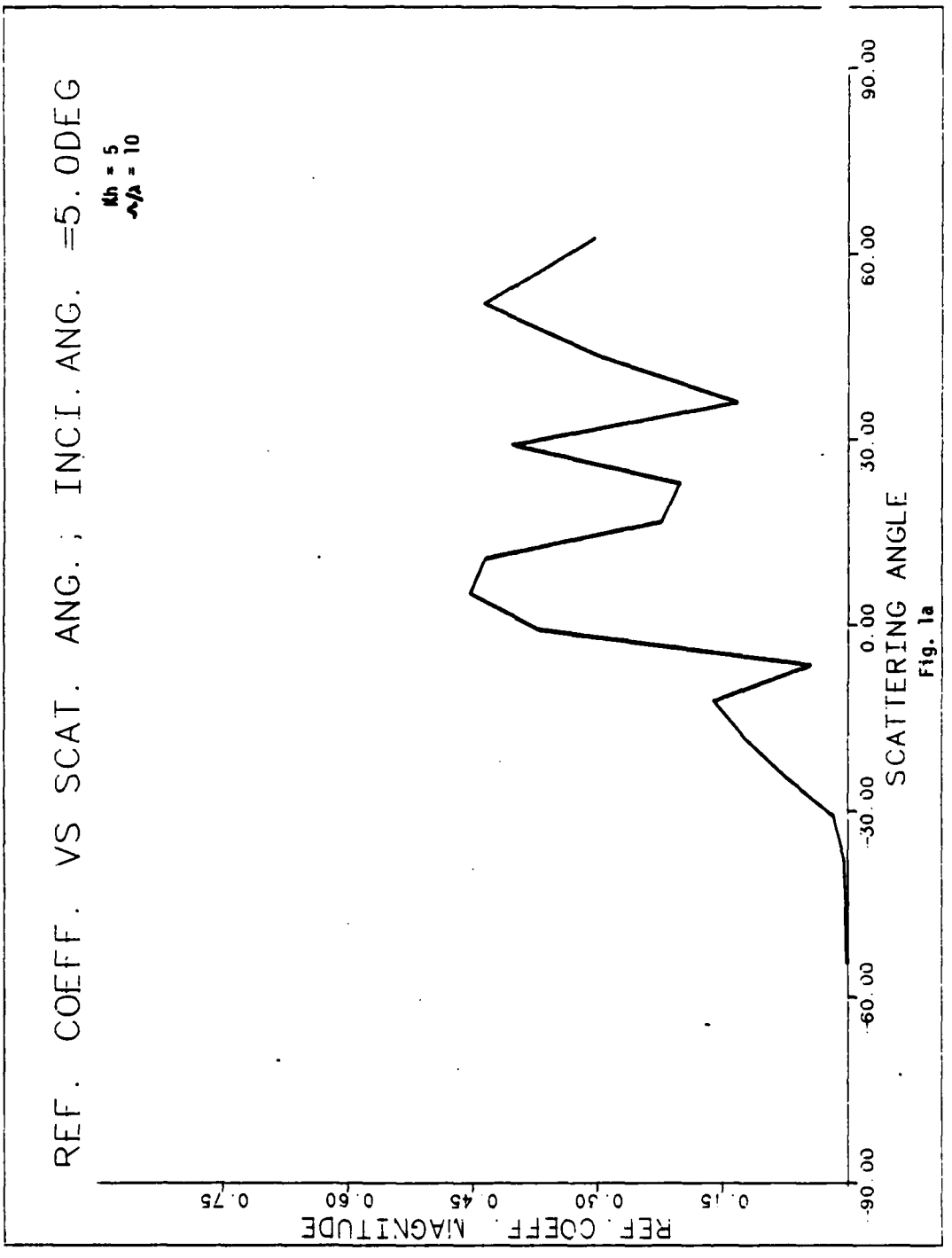
REF. COEFF. VS SCAT. ANG.; INCI. ANG. =5.0DEG
kh = 5
a/λ = 10
REF. COEFF. MAGNITUDE
0.15
0.30
0.45
0.60
0.75
-90.00
-60.00
-30.00
0.00
30.00
60.00
90.00
SCATTERING ANGLE

Fig. 1a

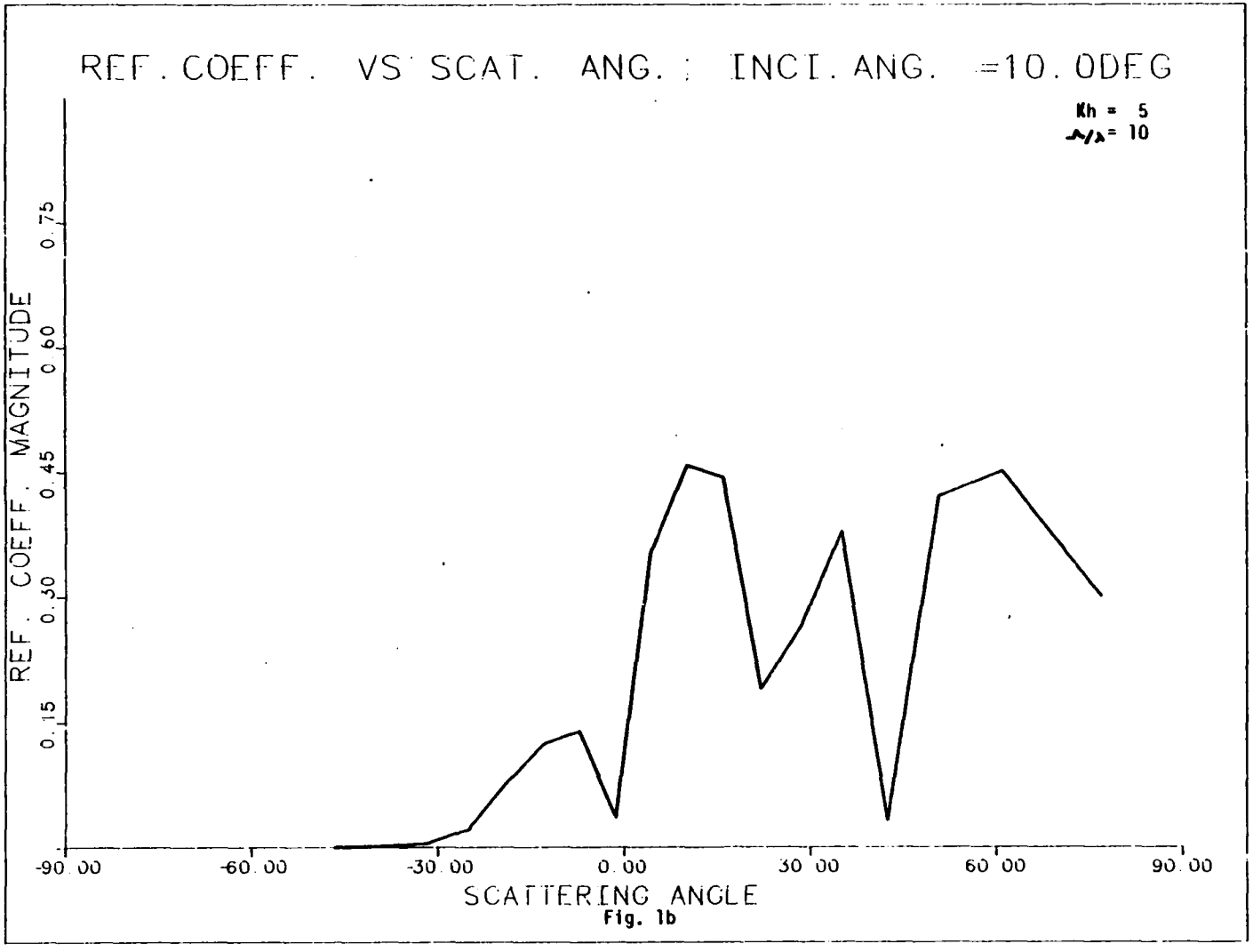
REF. COEFF. VS SCAT. ANG. ; INCI. ANG. =10.0DEG
Kh = 5
~/λ = 10
REF. COEFF. MAGNITUDE
0.15
0.30
0.45
0.60
0.75
-90.00
-60.00
-30.00
0.00
30.00
60.00
90.00
SCATTERING ANGLE
Fig. 1b

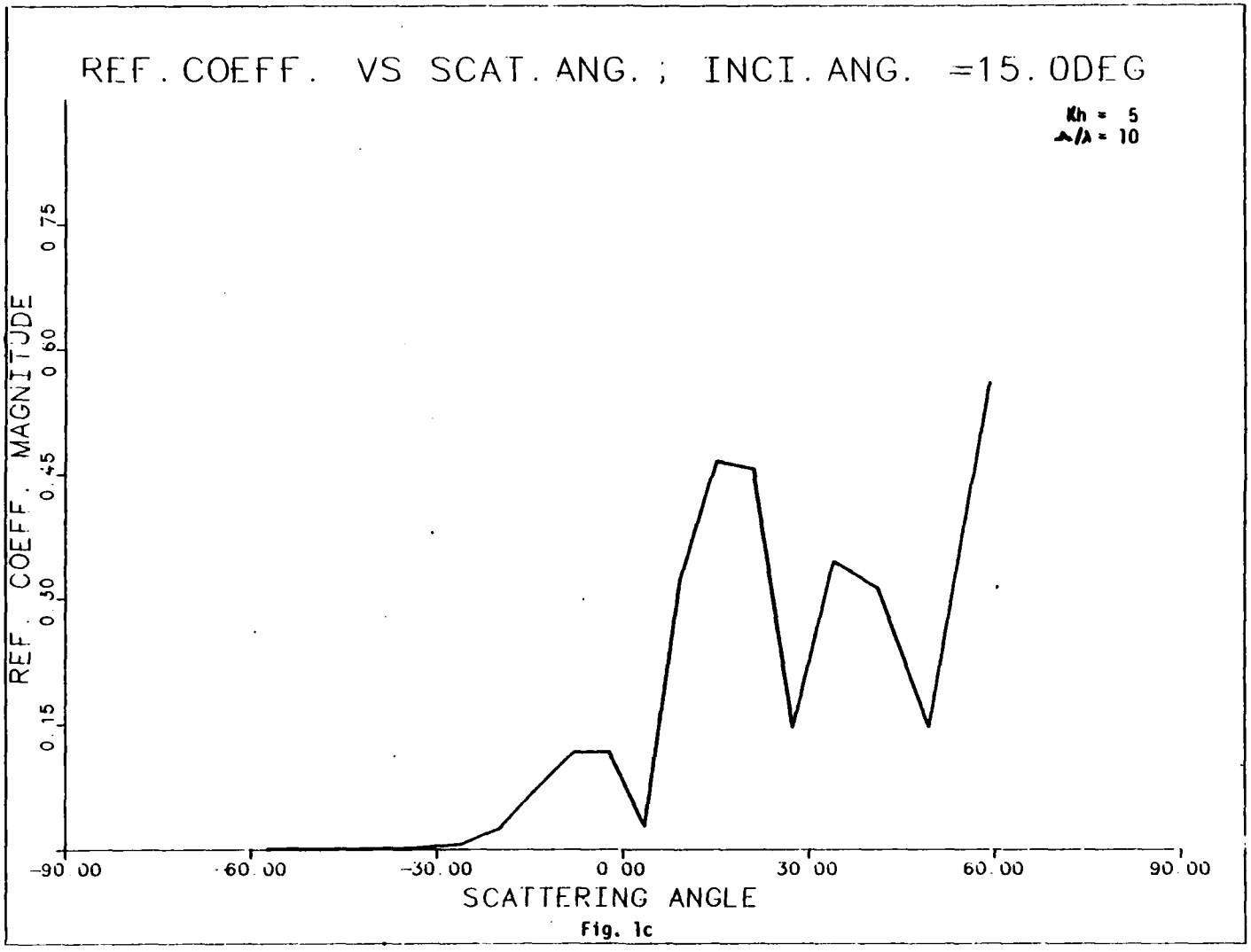
REF. COEFF. VS SCAT. ANG. ; INCI. ANG. =15. 0DEG
Kh = 5
λ/λ = 10
REF. COEFF. MAGNITUDE
0.15
0.30
0.45
0.60
0.75
-90.00
-60.00
-30.00
0.00
30.00
60.00
90.00
SCATTERING ANGLE

Fig. 1c

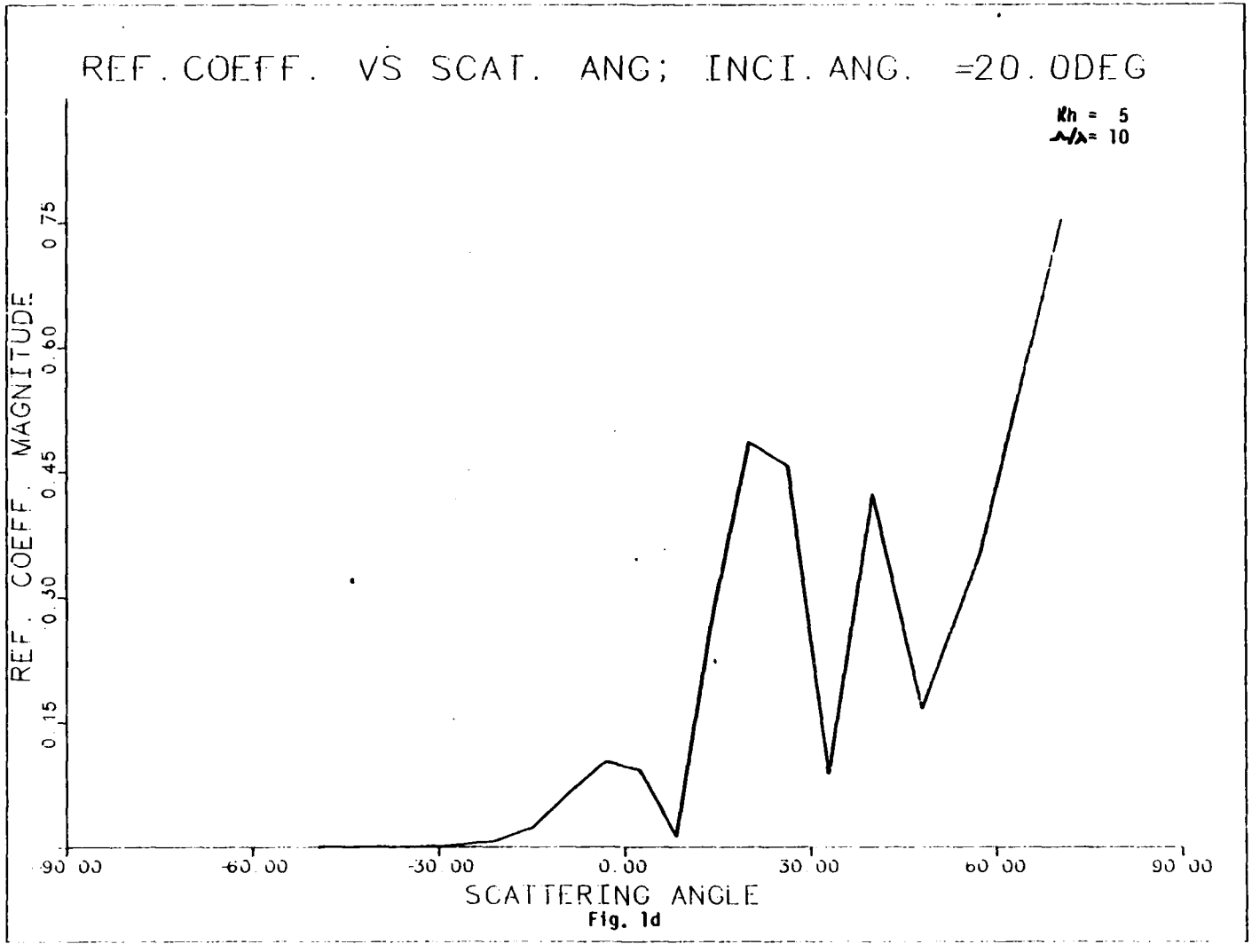
REF. COEFF. VS SCAT. ANG; INCI. ANG. =20.0DEG
Kh = 5
~/λ= 10
REF. COEFF. MAGNITUDE
0.15
0.30
0.45
0.60
0.75
-90.00
-60.00
-30.00
0.00
30.00
60.00
90.00
SCATTERING ANGLE
Fig. 1d

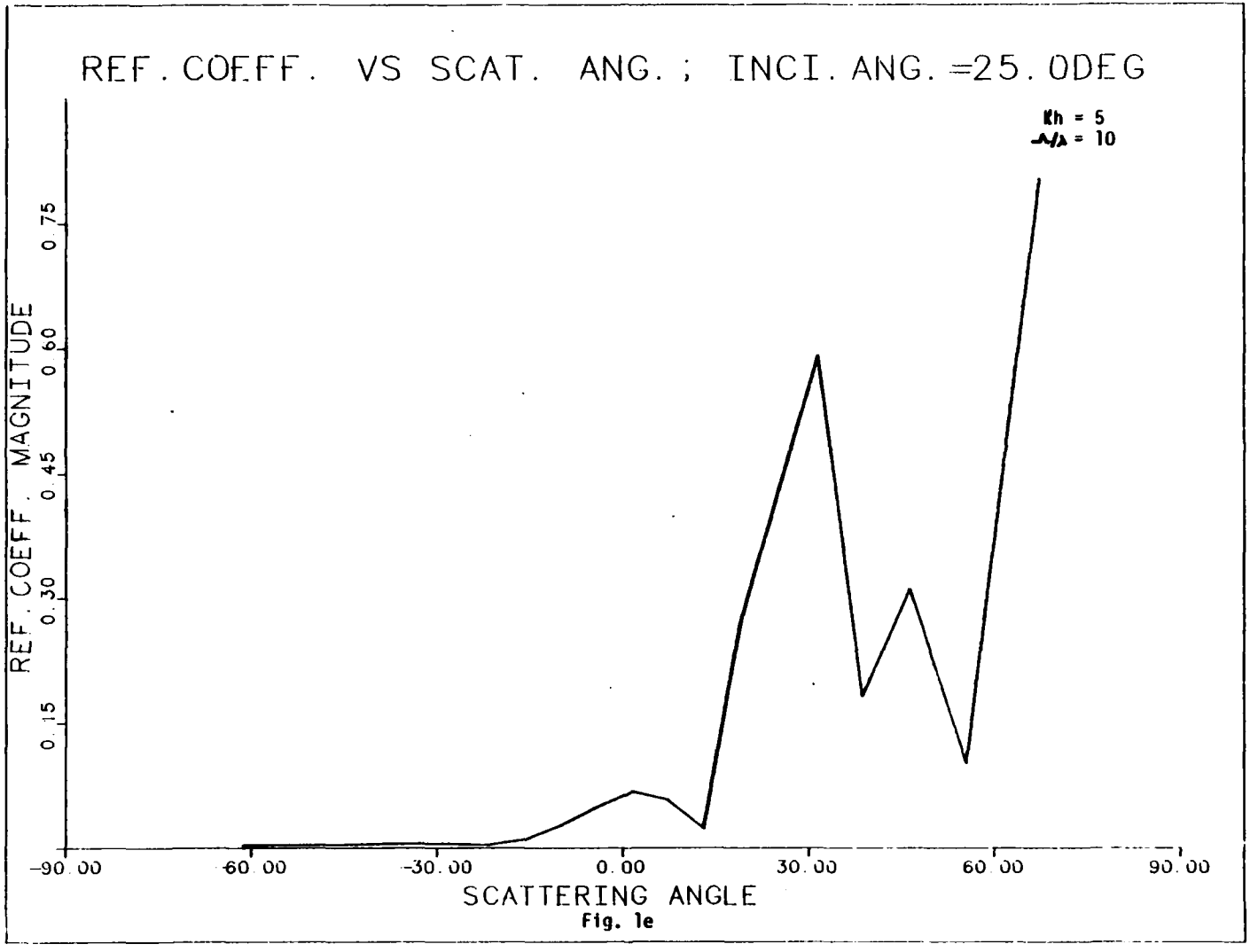
REF. COEFF. VS SCAT. ANG. ; INCI. ANG. =25. 0DEG
Kh = 5
λ/λ = 10
REF. COEFF. MAGNITUDE
0.15
0.30
0.45
0.60
0.75
-90.00
-60.00
-30.00
0.00
30.00
60.00
90.00
SCATTERING ANGLE

Fig. 1e

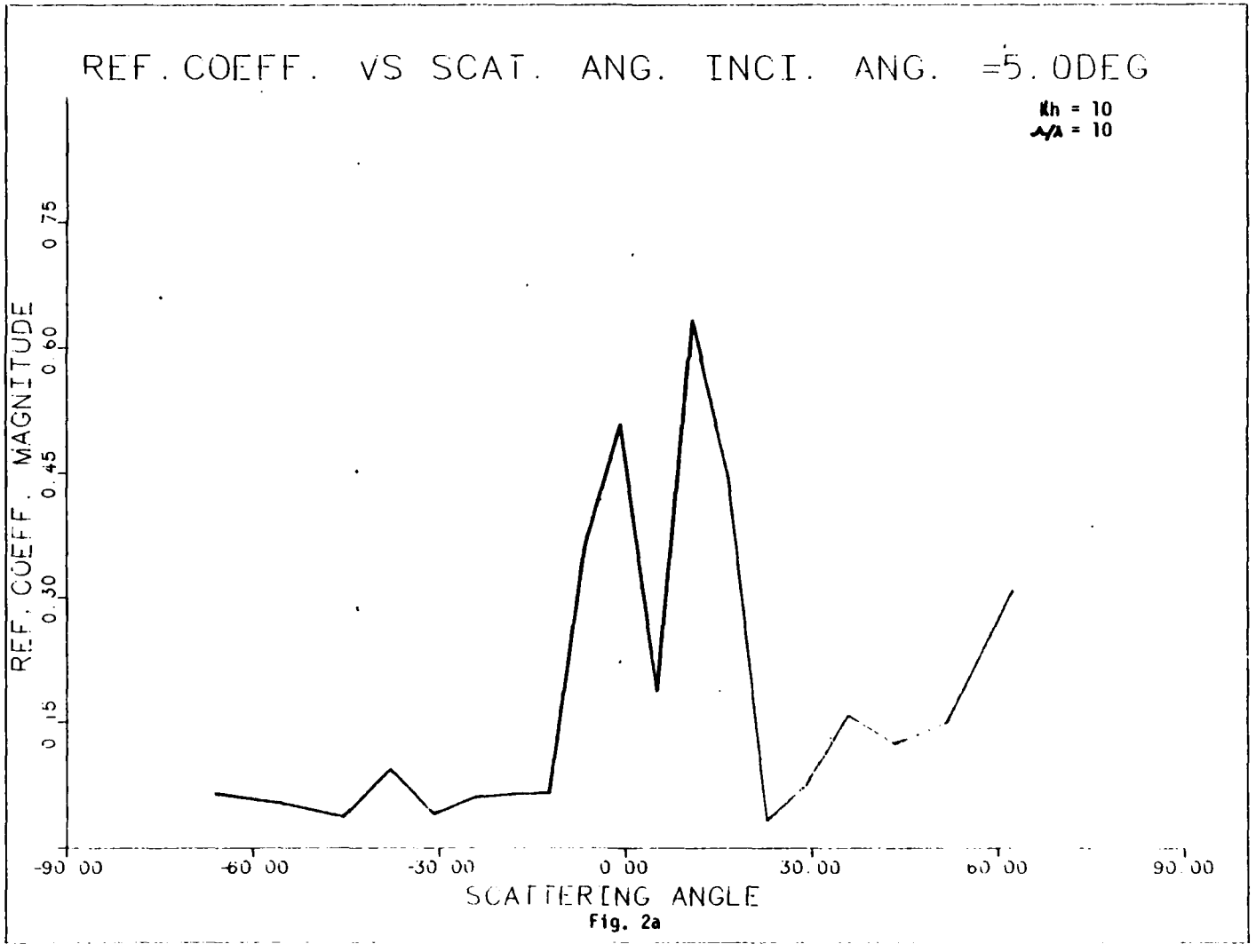
REF. COEFF. VS SCAT. ANG. INCI. ANG. =5.0DEG
Kh = 10
Ka = 10
REF. COEFF. MAGNITUDE
0.15
0.30
0.45
0.60
0.75
-90.00
-60.00
-30.00
0.00
30.00
60.00
90.00
SCATTERING ANGLE

Fig. 2a

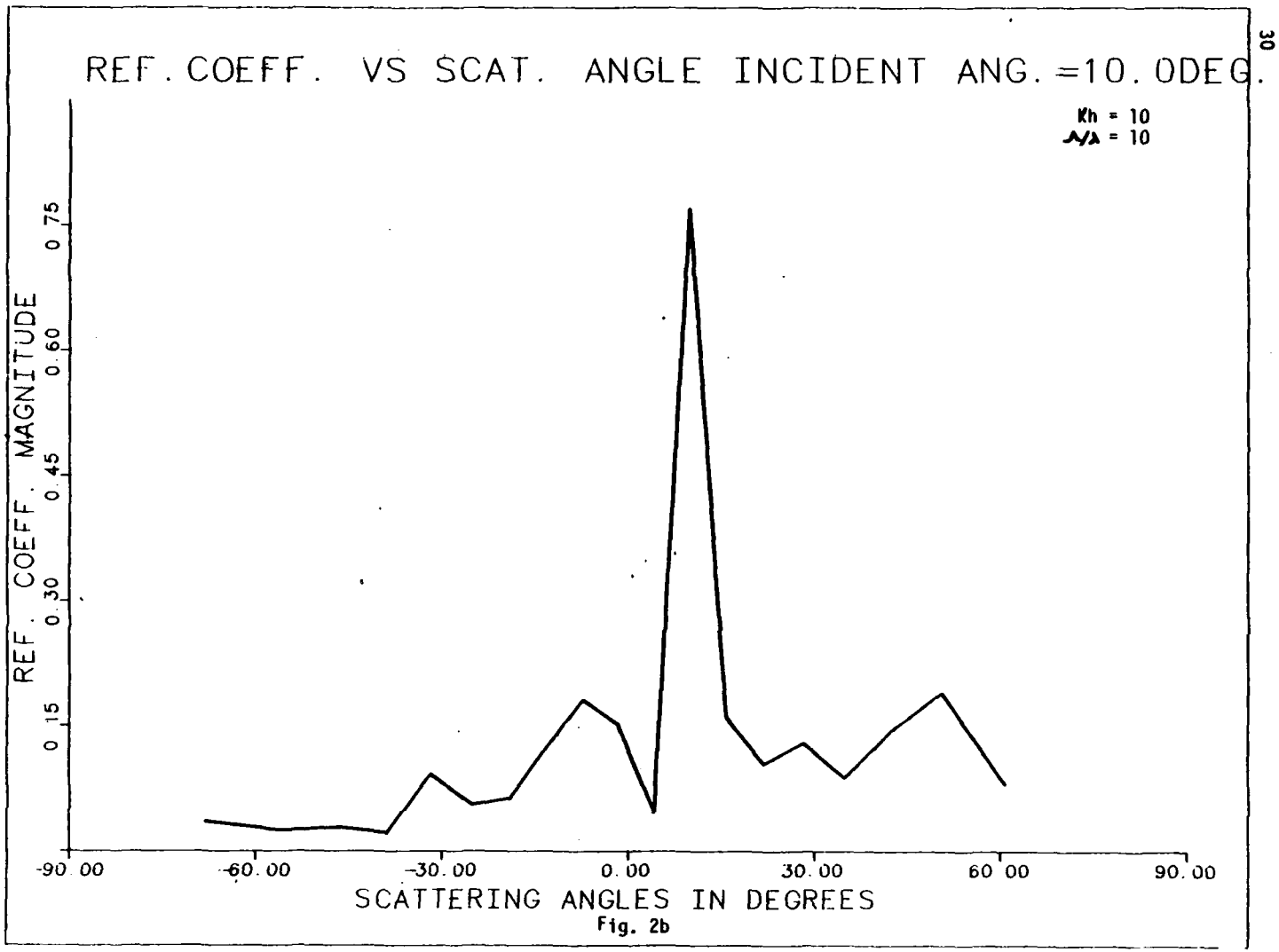
REF. COEFF. VS SCAT. ANGLE INCIDENT ANG. =10. 0DEG.
Kh = 10
N/λ = 10
REF. COEFF. MAGNITUDE
0.15
0.30
0.45
0.60
0.75
-90.00
-60.00
-30.00
0.00
30.00
60.00
90.00
SCATTERING ANGLES IN DEGREES
Fig. 2b

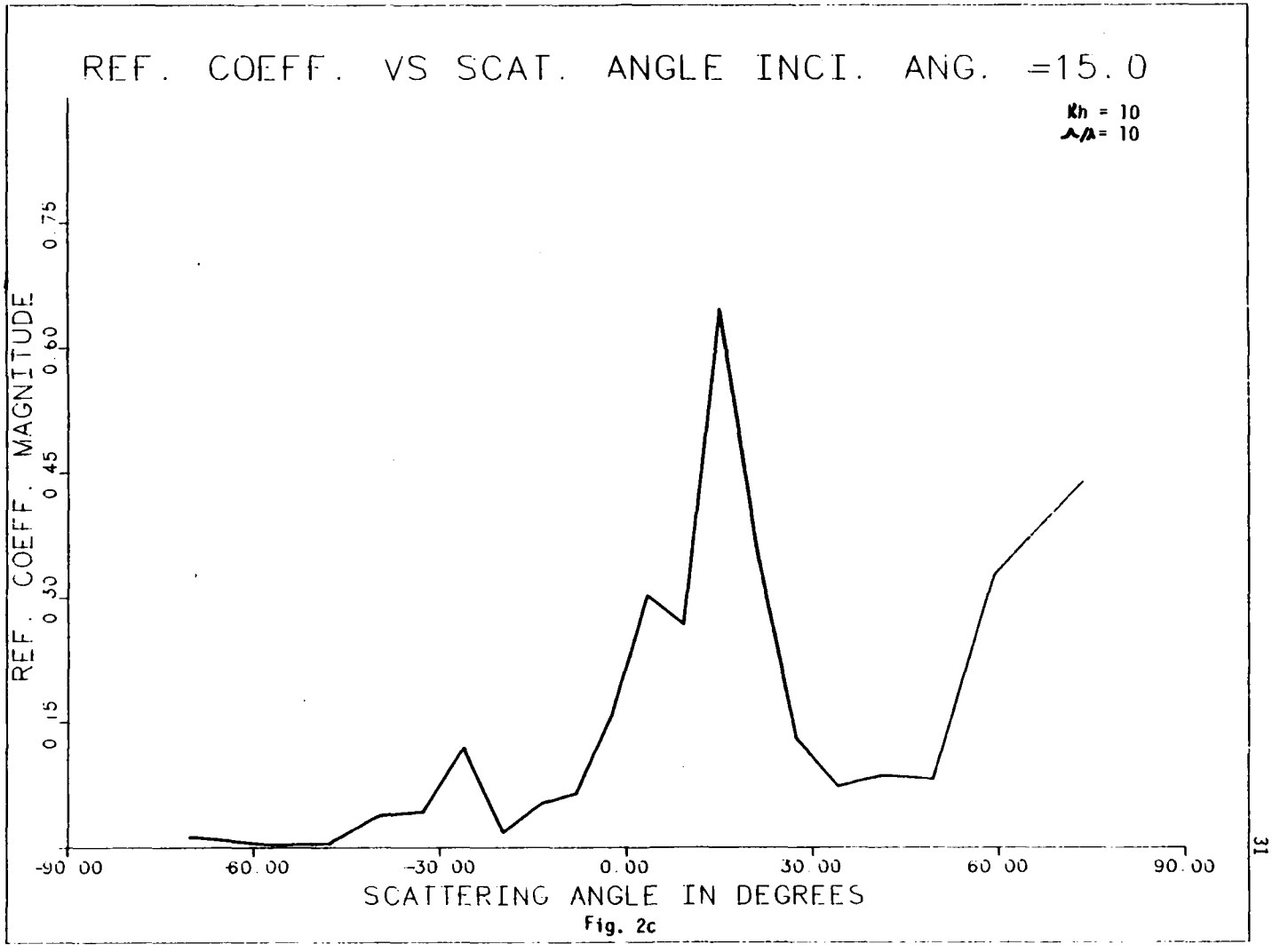
REF. COEFF. VS SCAT. ANGLE INCI. ANG. =15.0
Kh = 10
λ/λ = 10
REF. COEFF. MAGNITUDE
0.15
0.30
0.45
0.60
0.75
-90.00
-60.00
-30.00
0.00
30.00
60.00
90.00
SCATTERING ANGLE IN DEGREES

Fig. 2c

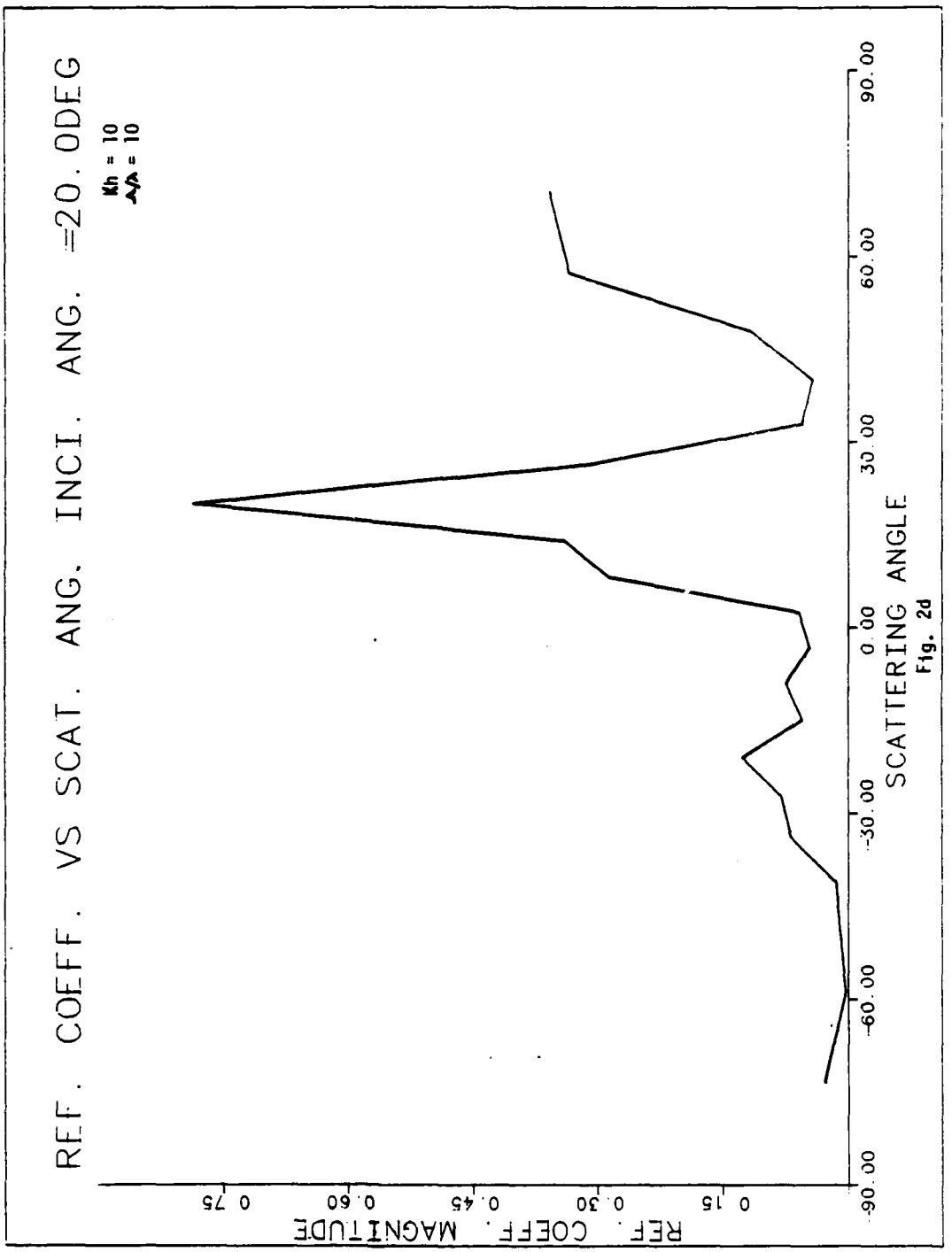
REF. COEFF. VS SCAT. ANG. INCI. ANG. =20.0DEG
kh = 10
kA = 10
REF. COEFF. MAGNITUDE
0.15
0.30
0.45
0.60
0.75
-90.00
-60.00
-30.00
0.00
30.00
60.00
90.00
SCATTERING ANGLE

Fig. 2d

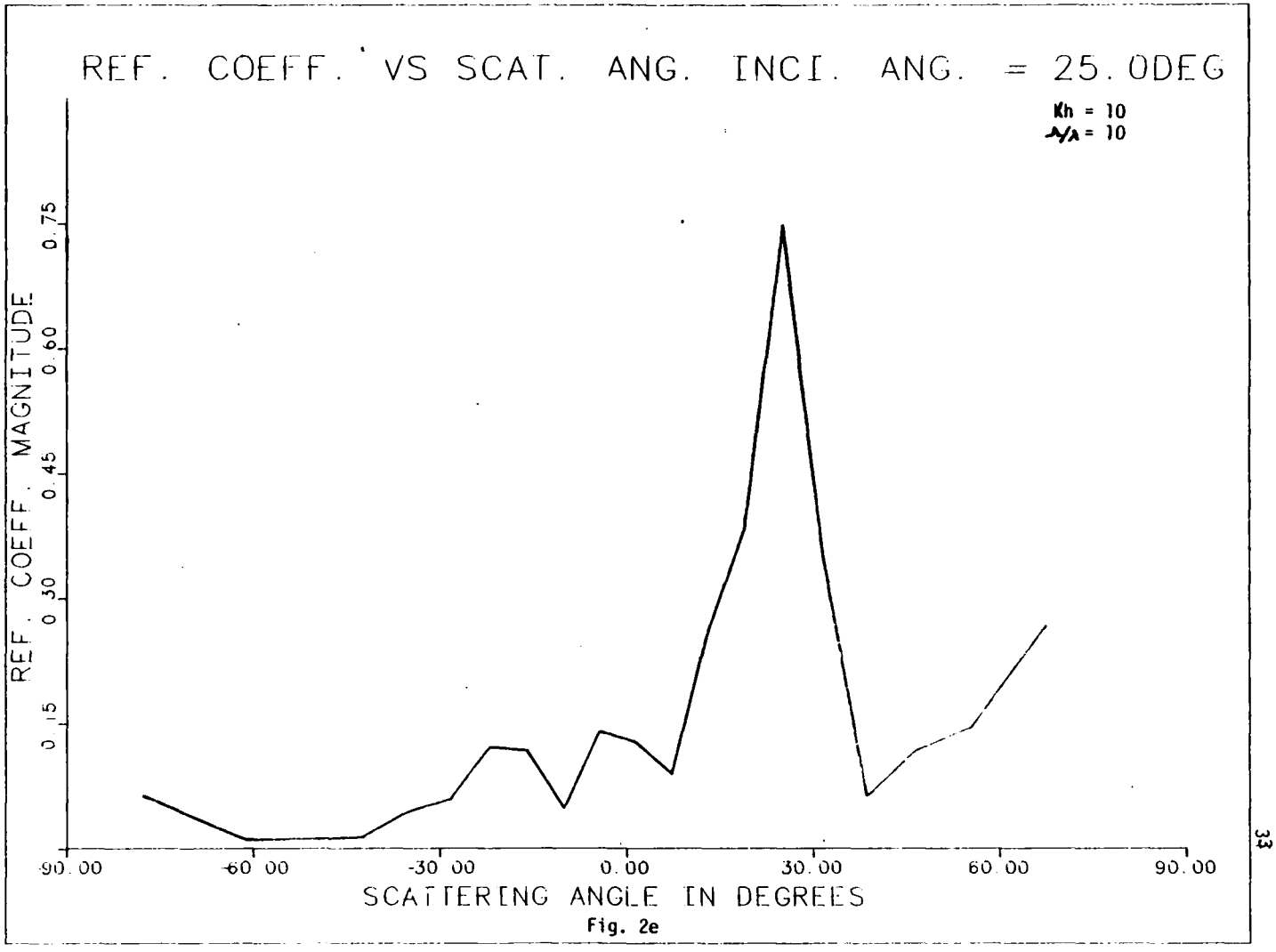
REF. COEFF. VS SCAT. ANG. INCI. ANG. = 25.0DEG
Kh = 10
A/λ = 10
REF. COEFF. MAGNITUDE
0.15
0.30
0.45
0.60
0.75
-90.00
-60.00
-30.00
0.00
30.00
60.00
90.00
SCATTERING ANGLE IN DEGREES

Fig. 2e

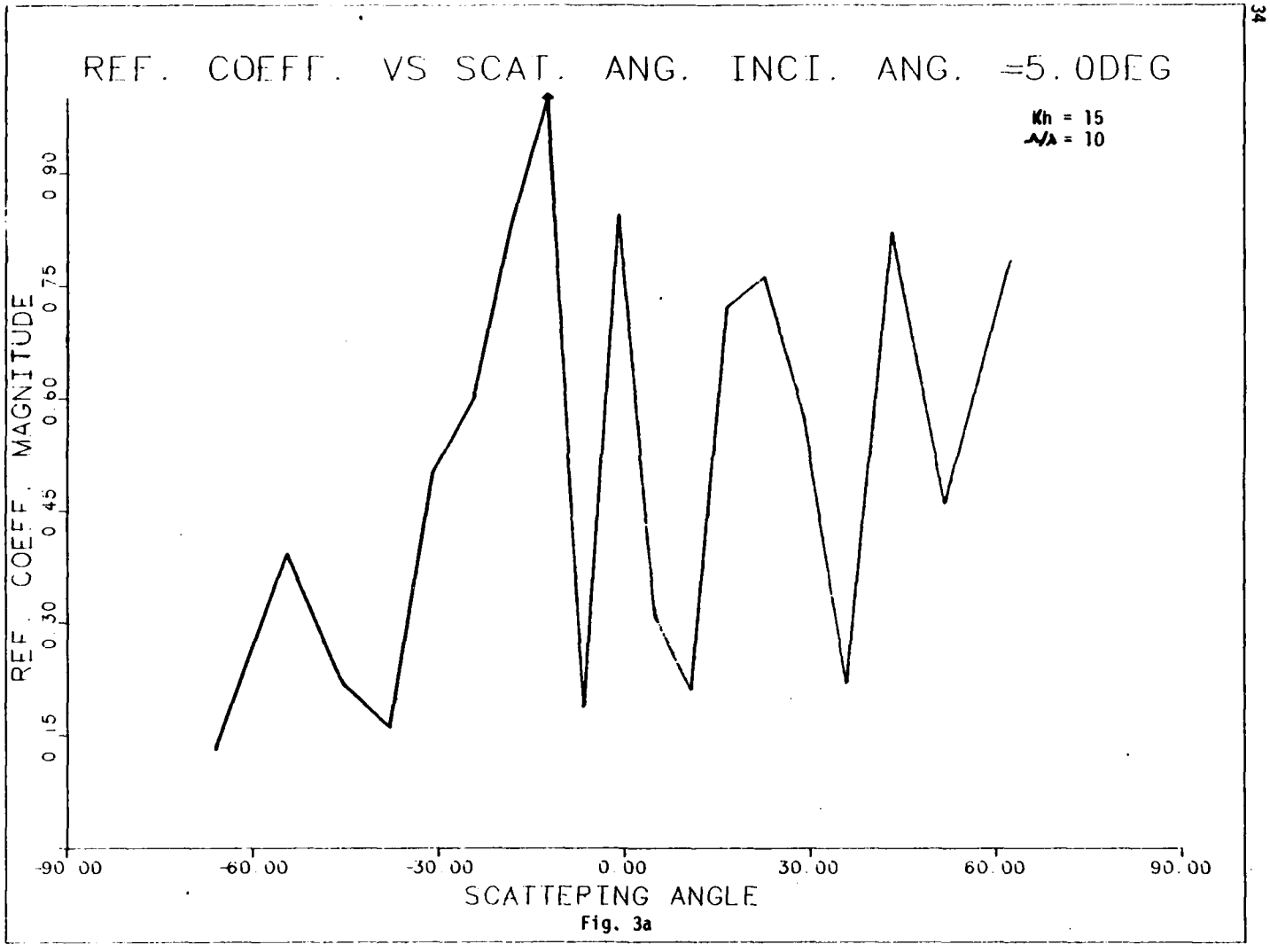
REF. COEFF. VS SCAT. ANG. INCI. ANG. =5.0DEG
Kh = 15
A/λ = 10
REF. COEFF. MAGNITUDE
0.15
0.30
0.45
0.60
0.75
0.90
-90.00
-60.00
-30.00
0.00
30.00
60.00
90.00
SCATTERING ANGLE

Fig. 3a

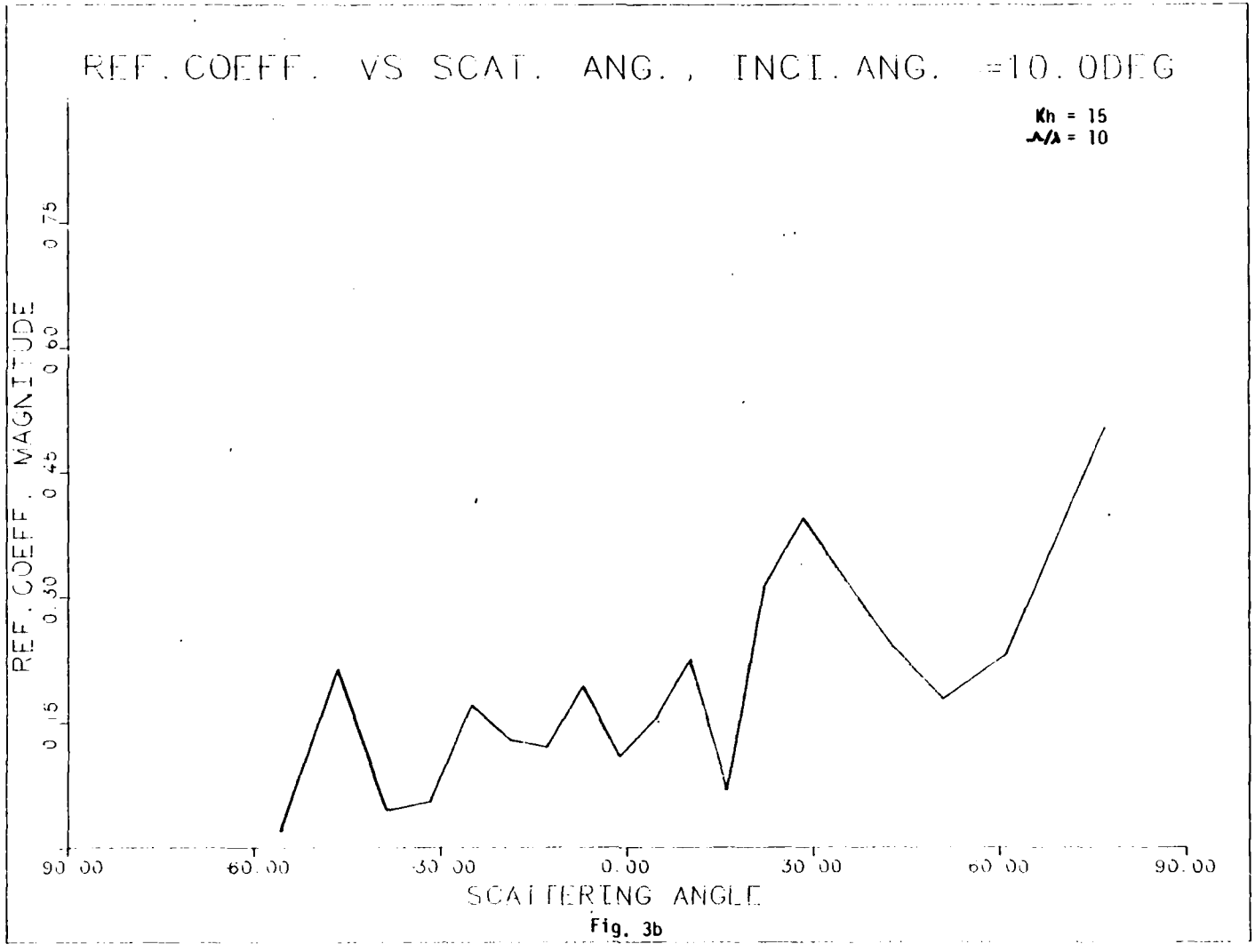
REF. COEFF. VS SCAT. ANG., INCI. ANG. =10.0DEG
Kh = 15
λ/λ = 10
REF. COEFF. MAGNITUDE
0.15
0.30
0.45
0.60
0.75
-90.00
-60.00
-30.00
0.00
30.00
60.00
90.00
SCATTERING ANGLE

Fig. 3b

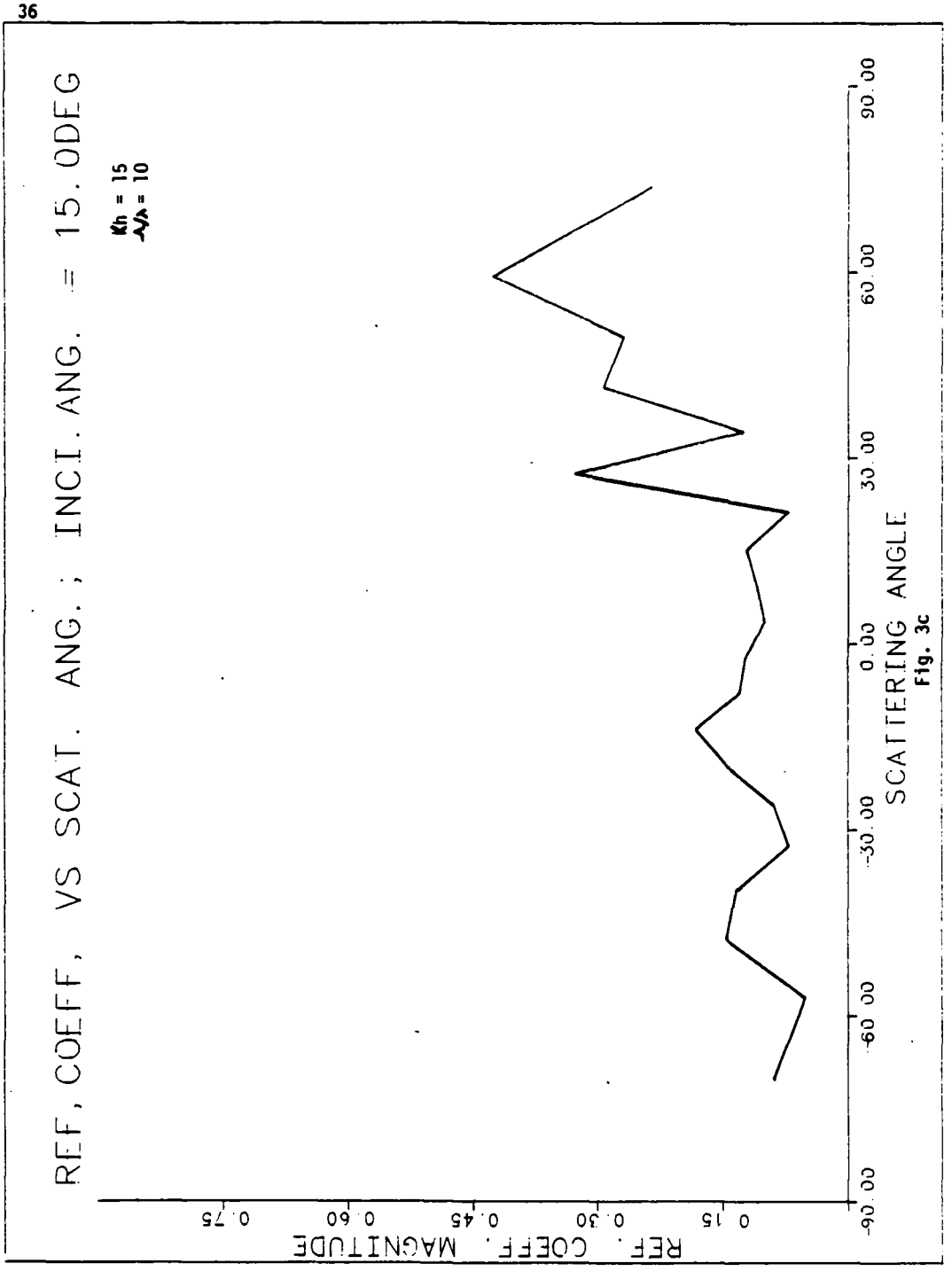
REF, COEFF, VS SCAT. ANG.; INCI. ANG. = 15.0DEG
kh = 15
a/λ = 10
REF. COEFF. MAGNITUDE
0.15
0.30
0.45
0.60
0.75
-90.00
-60.00
-30.00
0.00
30.00
60.00
90.00
SCATTERING ANGLE

Fig. 3c

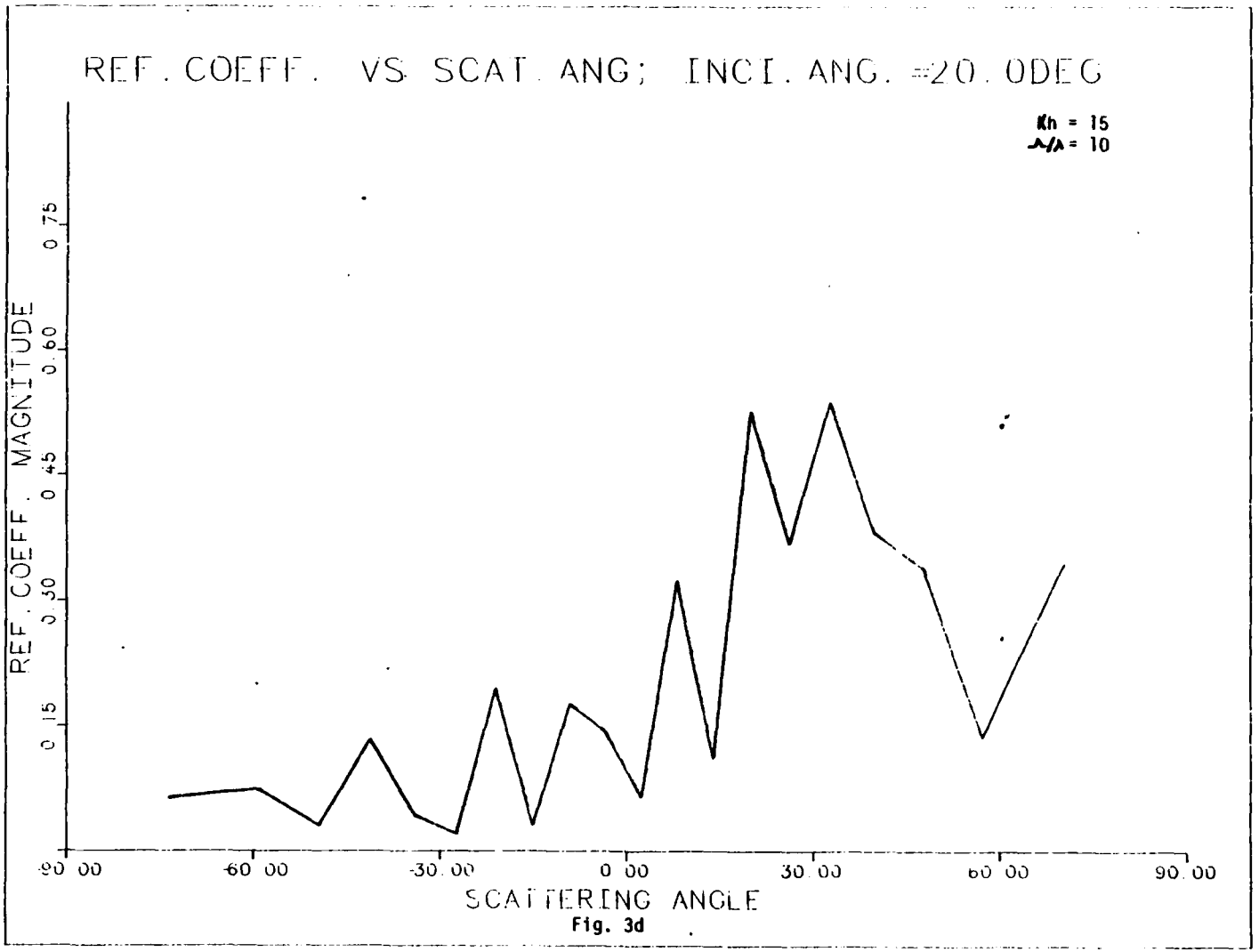
REF. COEFF. VS SCAT. ANG; INCI. ANG. =20.0DEG
Kh = 15
λ/λ = 10
REF. COEFF. MAGNITUDE
0.75
0.60
0.45
0.30
0.15
-90.00
-60.00
-30.00
0.00
30.00
60.00
90.00
SCATTERING ANGLE
Fig. 3d

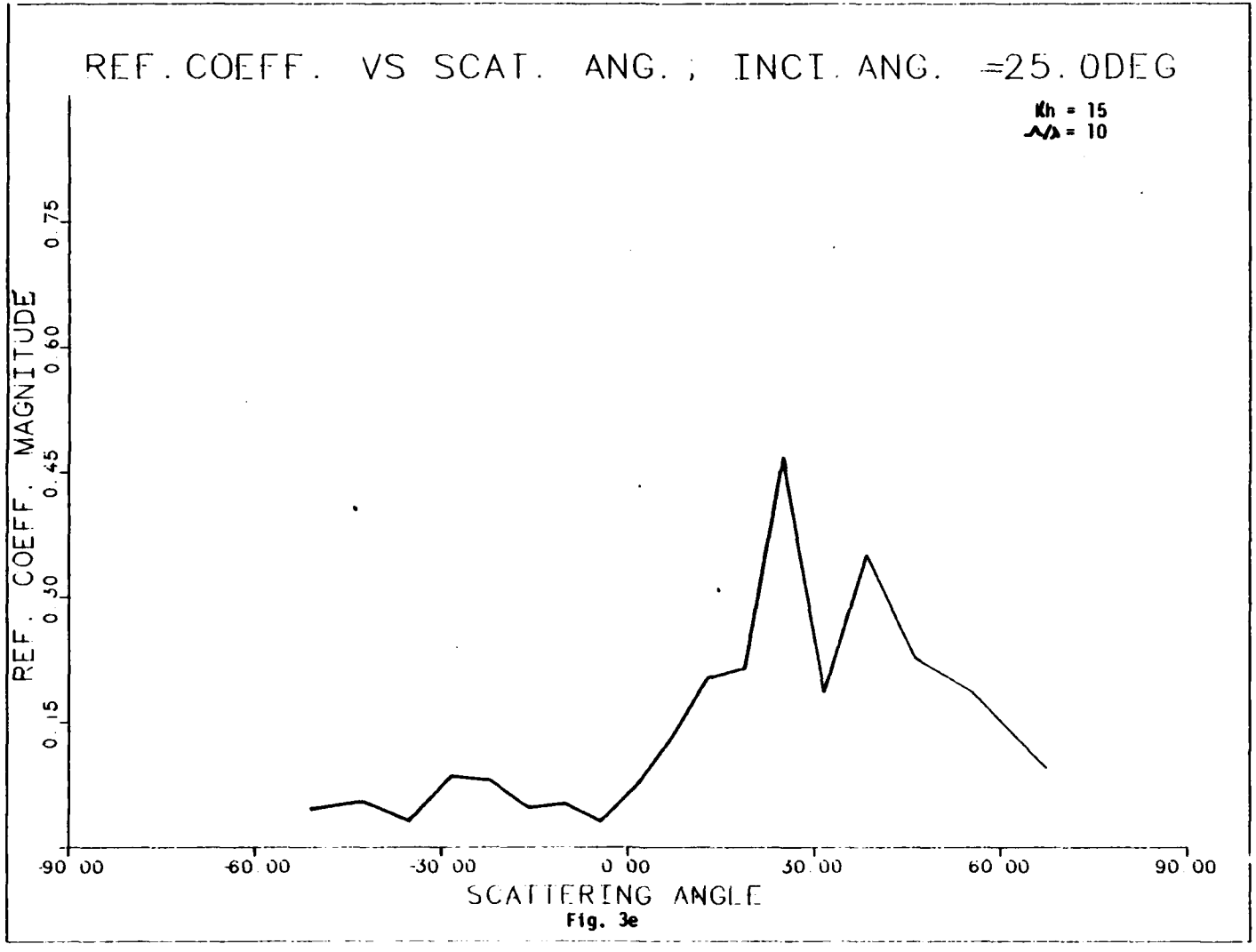
REF. COEFF. VS SCAT. ANG. ; INCI. ANG. =25.0DEG
Kh = 15
Ka = 10
REF. COEFF. MAGNITUDE
0.15
0.30
0.45
0.60
0.75
-90.00
-60.00
-30.00
0.00
30.00
60.00
90.00
SCATTERING ANGLE

Fig. 3e

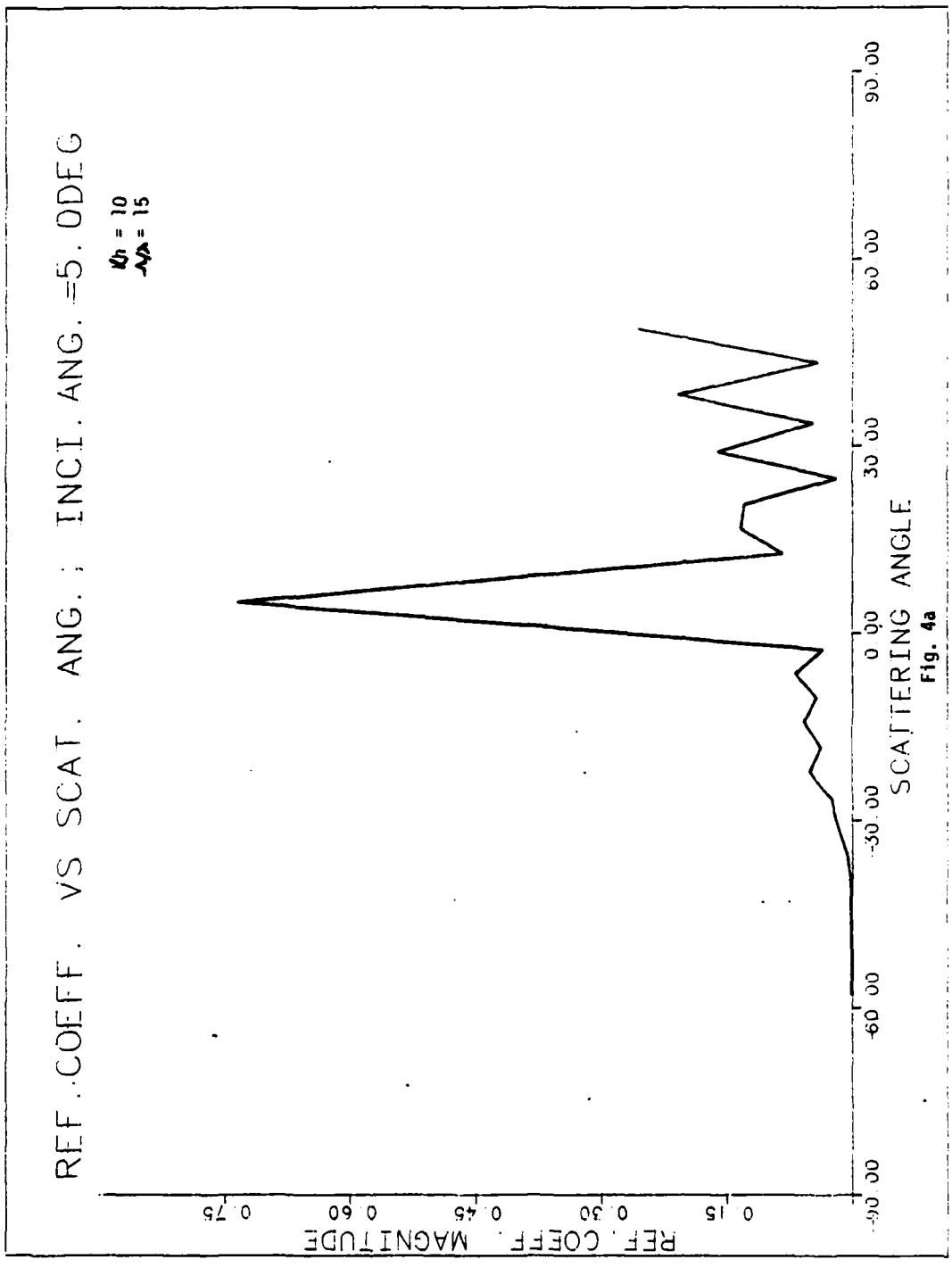
REF. COEFF. VS SCAT. ANG. ; INCI. ANG. =5. 0DEG
$k_h$ = 10
$k_\phi$ = 15
REF. COEFF. MAGNITUDE
0.15
0.30
0.45
0.60
0.75
-90.00
-60.00
-30.00
0.00
30.00
60.00
90.00
SCATTERING ANGLE

Fig. 4a

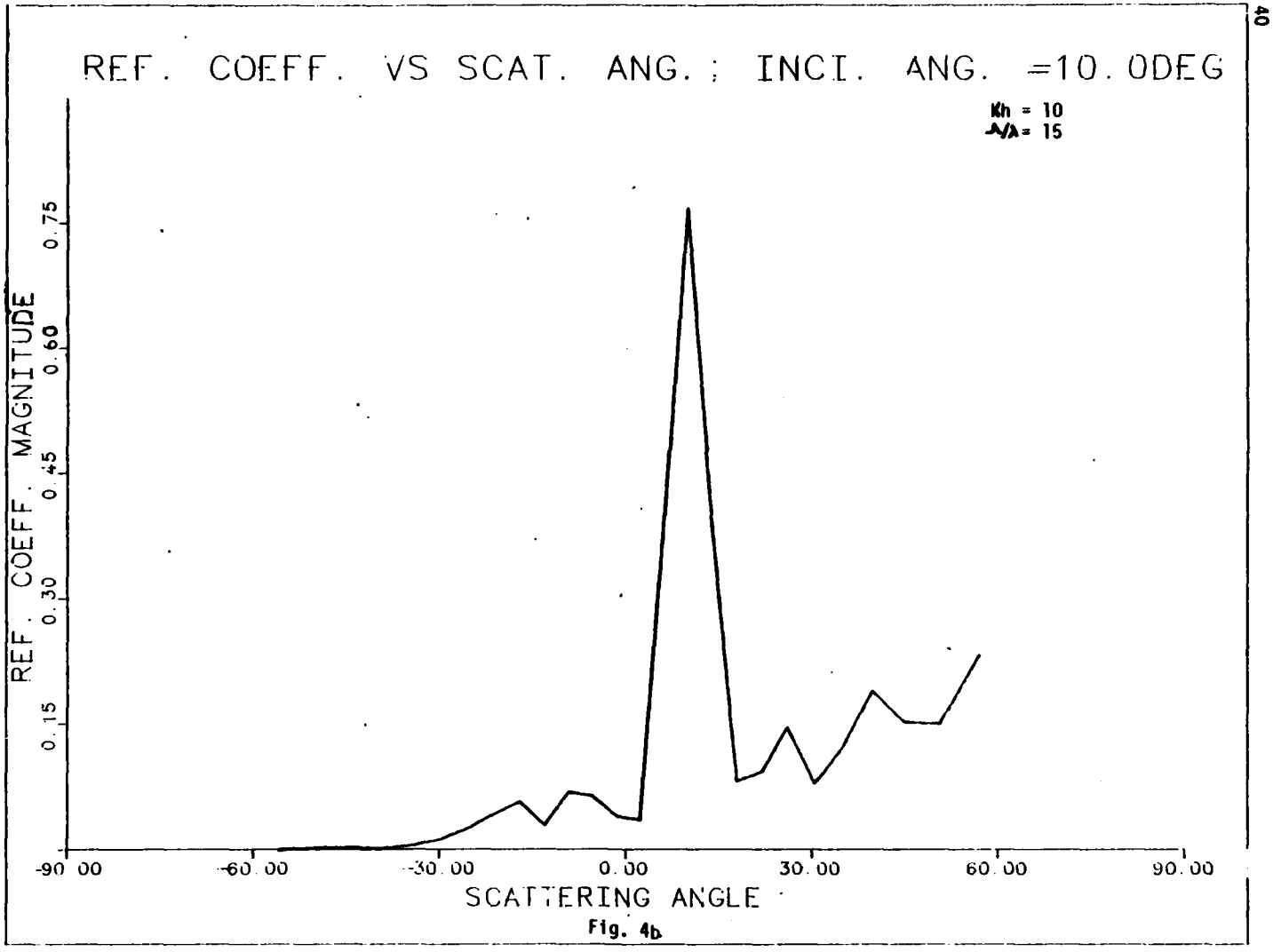
REF. COEFF. VS SCAT. ANG.; INCI. ANG. =10.0DEG
Kh = 10
A/λ = 15
REF. COEFF. MAGNITUDE
0.15
0.30
0.45
0.60
0.75
-90.00
-60.00
-30.00
0.00
30.00
60.00
90.00
SCATTERING ANGLE

Fig. 4b

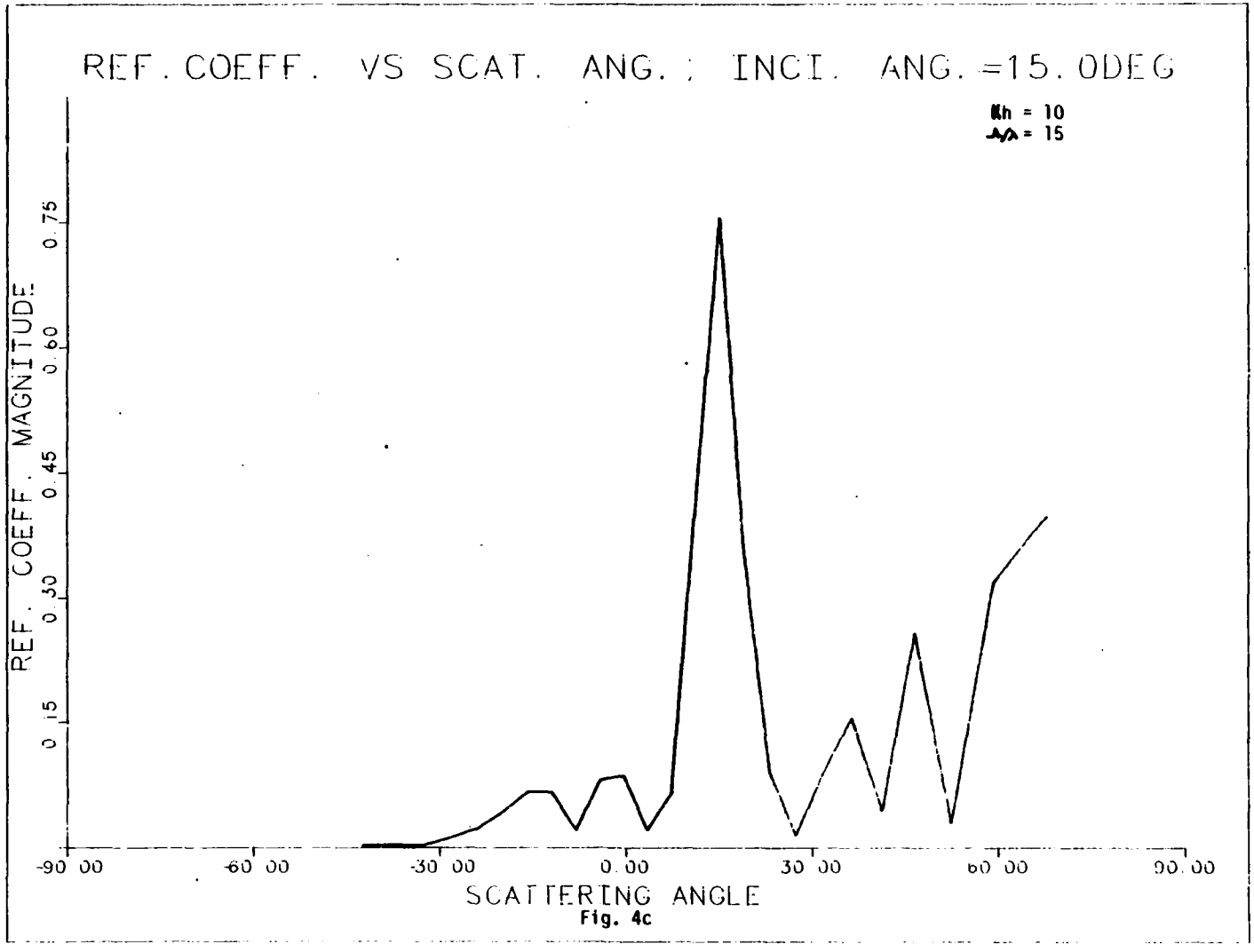
REF. COEFF. VS SCAT. ANG. ; INCI. ANG. =15. 0DEG
Kh = 10
Ka = 15
REF. COEFF. MAGNITUDE
0.15
0.30
0.45
0.60
0.75
-90.00
-60.00
-30.00
0.00
30.00
60.00
90.00
SCATTERING ANGLE

Fig. 4c

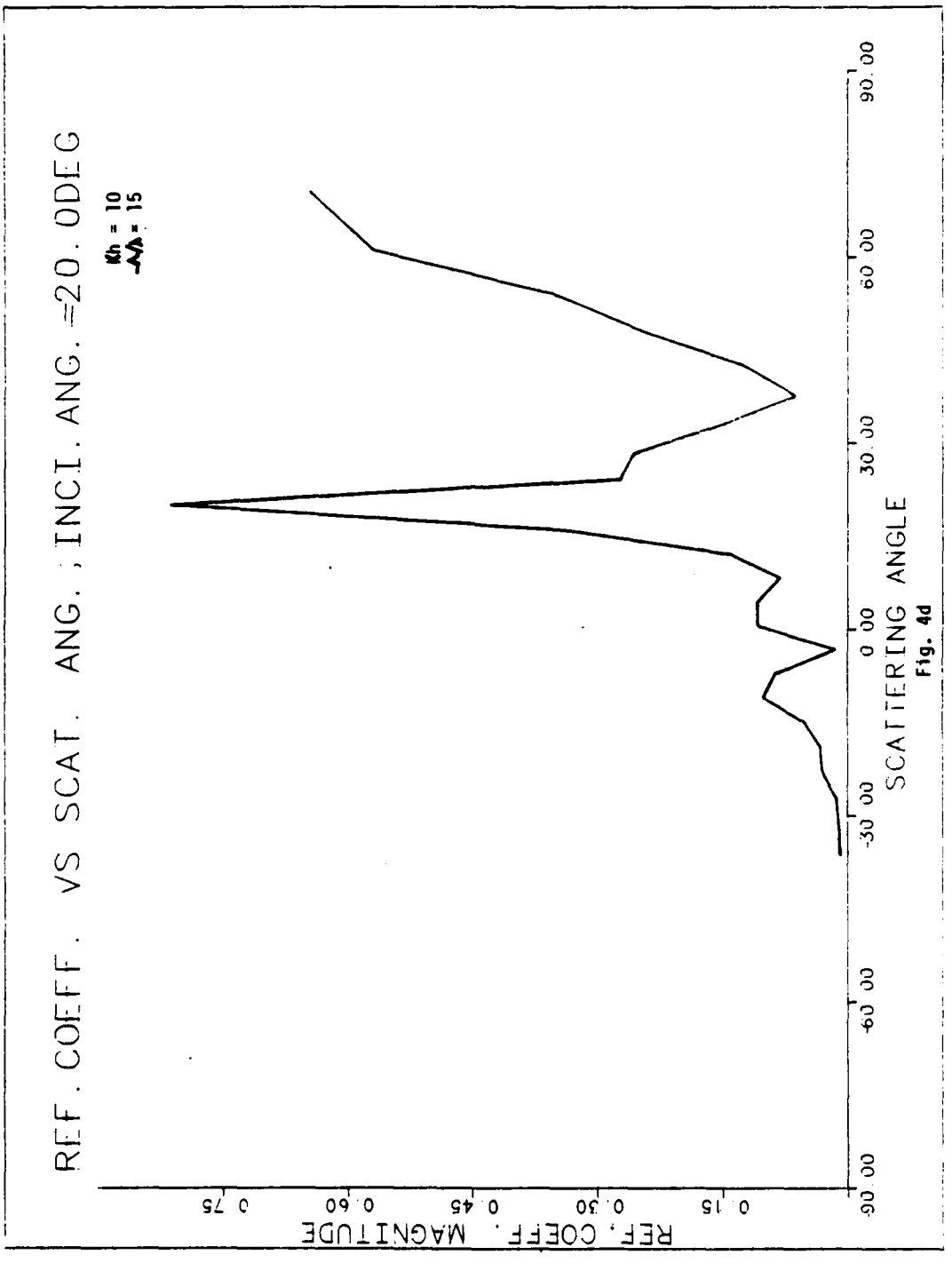
REF. COEFF. VS SCAT. ANG., INCI. ANG. =20.0DEG
kh = 10
λ/h = 15
REF. COEFF. MAGNITUDE
0.15
0.30
0.45
0.60
0.75
-90.00
-60.00
-30.00
0.00
30.00
60.00
90.00
SCATTERING ANGLE

Fig. 4d

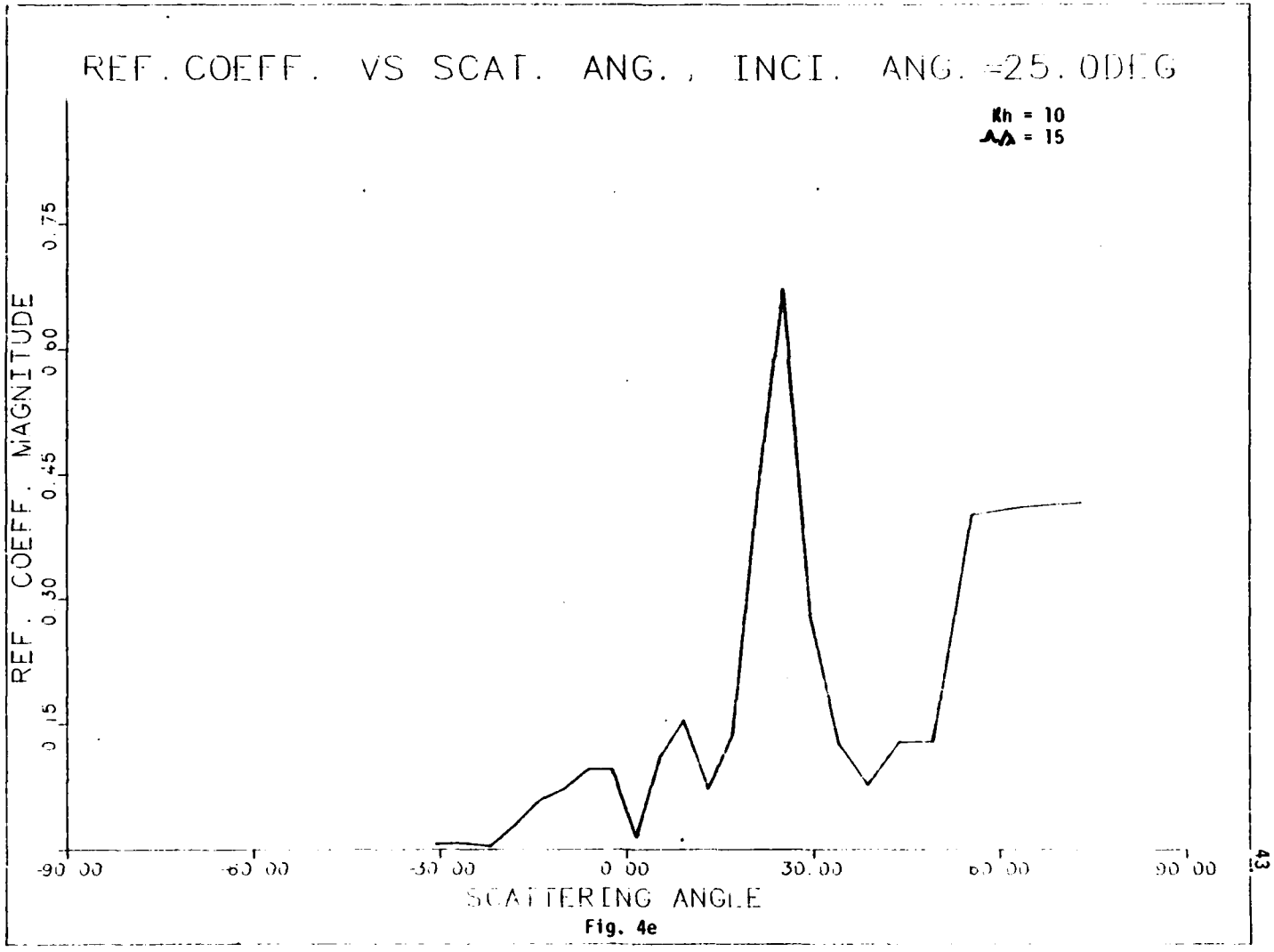
REF. COEFF. VS SCAT. ANG., INCI. ANG. =25.0DEG
Kh = 10
λ/λ = 15
REF. COEFF. MAGNITUDE
0.15
0.30
0.45
0.60
0.75
-90.00
-60.00
-30.00
0.00
30.00
60.00
90.00
SCATTERING ANGLE

Fig. 4e

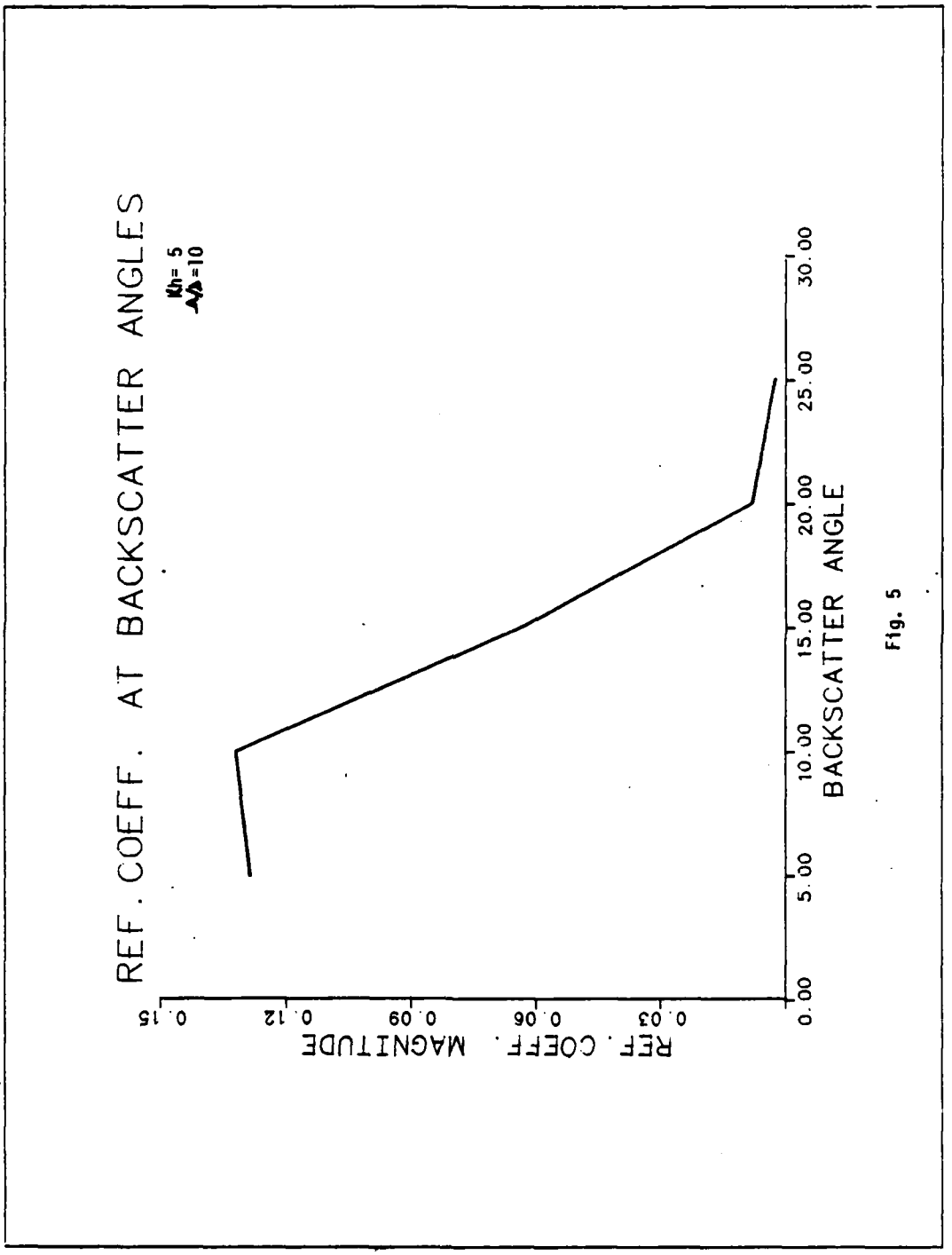
REF. COEFF. AT BACKSCATTER ANGLES
Kh= 5
Ka=10
REF. COEFF. MAGNITUDE
0.00
0.03
0.06
0.09
0.12
0.15
0.00
5.00
10.00
15.00
20.00
25.00
30.00
BACKSCATTER ANGLE

Fig. 5

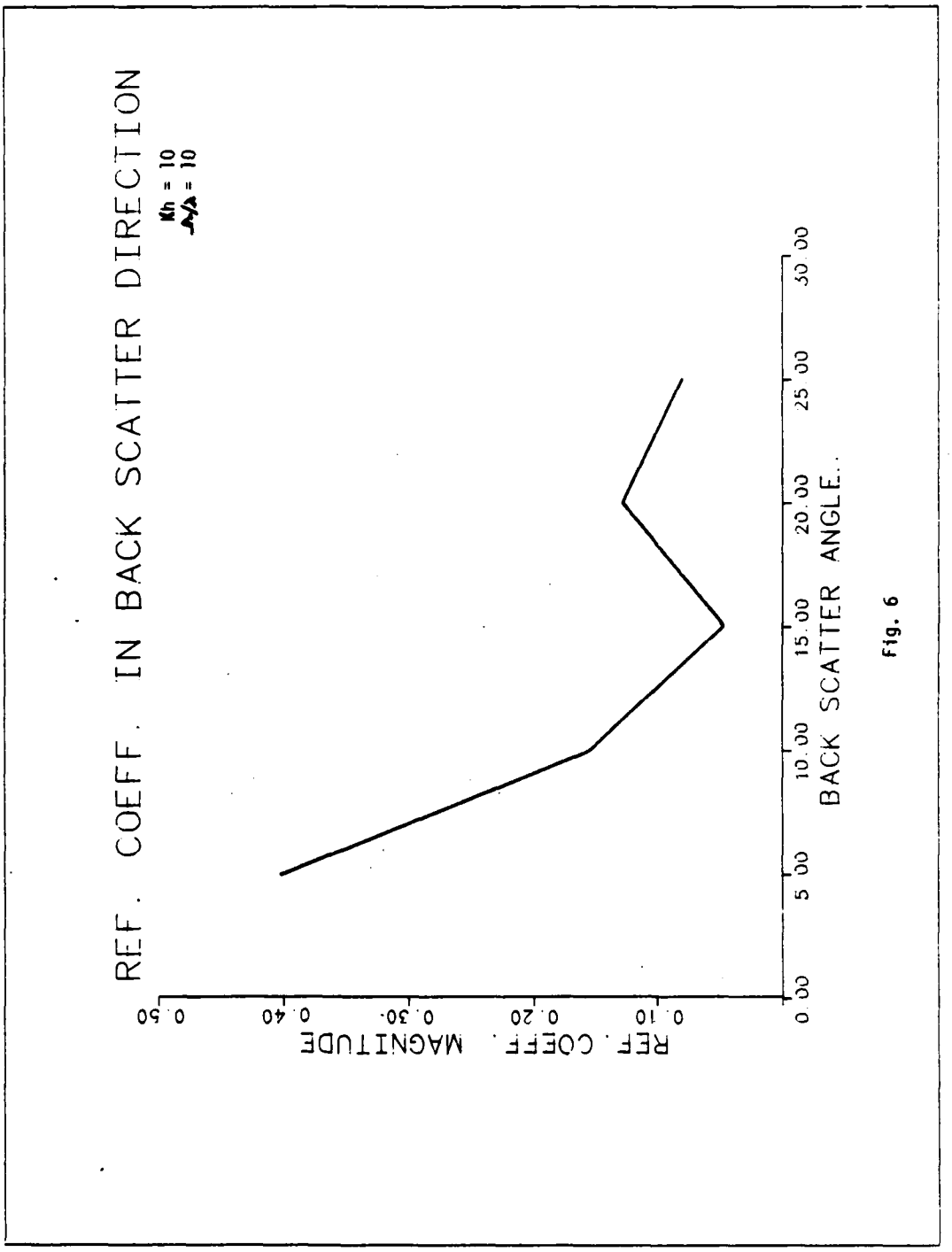
REF. COEFF. IN BACK SCATTER DIRECTION
kh = 10
kA = 10
REF. COEFF. MAGNITUDE
0.00
0.10
0.20
0.30
0.40
0.50
5.00
10.00
15.00
20.00
25.00
30.00
BACK SCATTER ANGLE..

Fig. 6

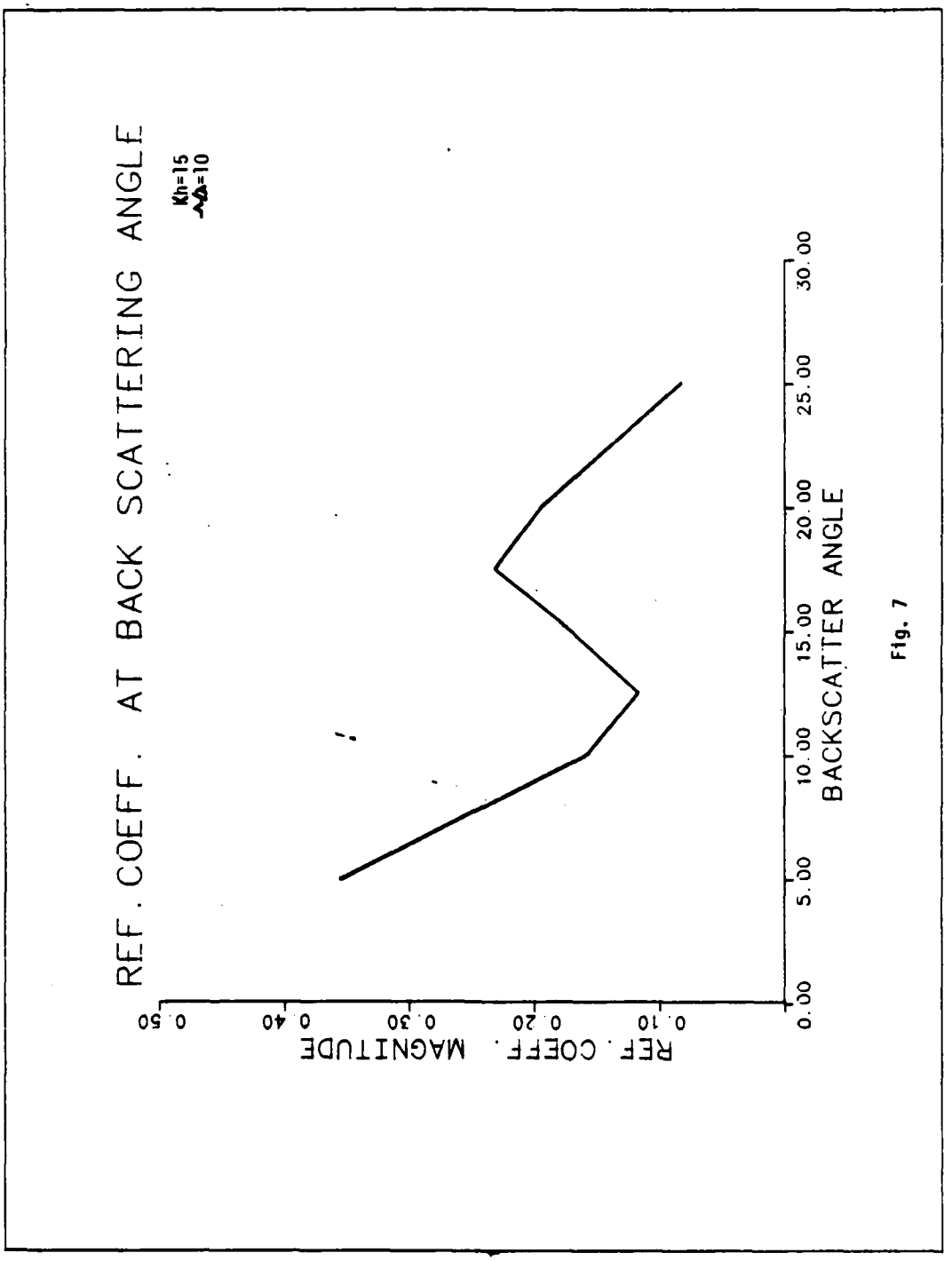
REF. COEFF. AT BACK SCATTERING ANGLE
Kh=15
Δ=10
REF. COEFF. MAGNITUDE
0.10
0.20
0.30
0.40
0.50
0.00
5.00
10.00
15.00
20.00
25.00
30.00
BACKSCATTER ANGLE

Fig. 7

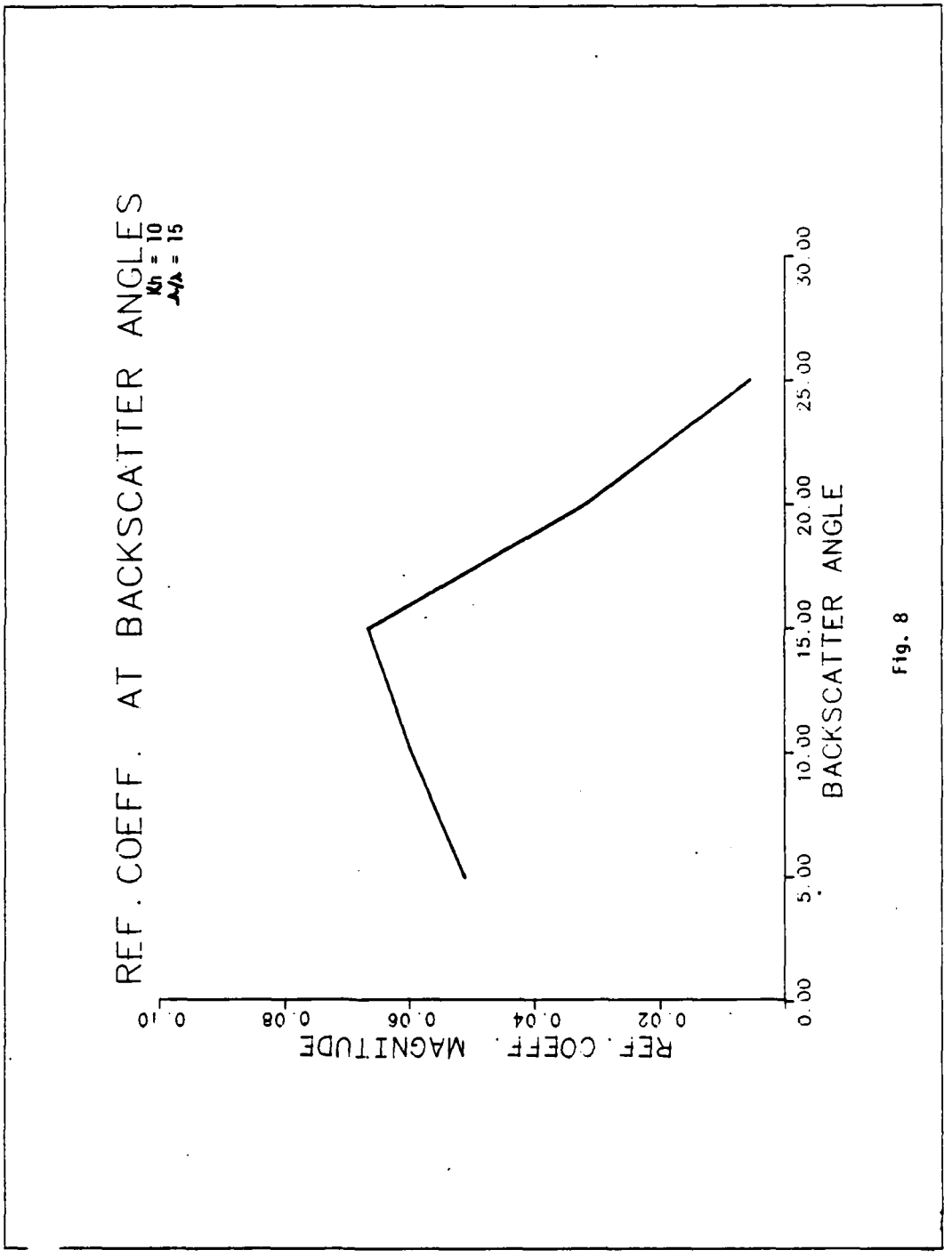
REF. COEFF. AT BACKSCATTER ANGLES
Kh = 10
kA = 15
REF. COEFF. MAGNITUDE
0.00
0.02
0.04
0.06
0.08
0.10
0.00
5.00
10.00
15.00
20.00
25.00
30.00
BACKSCATTER ANGLE

Fig. 8

vergent results

(b) Nyquist criteria was used for sampling while performing the 2-D FFT.

(c) A rectangular window for the FFT did not perform well, while Hanning window significantly improved the results.

(d) Conservation of energy was used as a test to check the validity of the results and except for one case, the energy conservation was not violated. In that case (5° angle), the reflection coefficient was slightly greater than one at scattering angles close to grazing and less than one at other angles.

Figures 1 to 4, the reflected energy is given as a function of the incident angle ($\theta$) for various scattered angles. The back scattered angle is $-\theta$. As the incident angle increases the back scattered intensity decreases significantly. Figure (5-7) shows the back scattered energy as a function of the incident angle for Kh = 5,10,15 and $\Lambda/\lambda$ = 10 and Figure 8 for Kh = 10 and $\Lambda/\lambda$ = 15. The back scattered energy decreases rapidly to insignificant levels beyond 25°. However it seems to be having a minimum between 0 and 25°. This may be a possible explanation for the observed variation in the intensity of the two SAR images in the LA area.

For the same Kh = 10, as $\Lambda/\lambda$ increases, (Figures 6 and 8) the reflected energy decreases significantly. This indicates that the fundamental component of the spatial structure contributes a significant amount of energy.

## IV. Conclusions and Recommendations

The numerical results indicate that there is a definite variation in the back scattered intensity as a function of the aspect angle. However in order for us to do a more realistic model, we would need the facilities of a large computer like the CRAY, due to the computer intensive nature of the calculation. In any future work, a request for such facilities has to be made, and only then can one compare the actual observations from the SeaSat images with the model calculations.

Modelling of the back scatter as being from a series of regularly spaced flat rectangular radiators parallel to the earth surface was not pursued as it was felt that significant errors would result from neglecting the height of the buildings. To include this effect, one would have to use some modified aspects of ray tracing and GTD corrections to rays. This represents another alternate approach that needs to be investigated and numerically implemented.

In order for us to get a more quantitative feel for the back scattered radiation, it would be useful to perform experiments on scaled down models using laser beams and optical frequencies. Measurements of optical backscatter can be made by modelling the city as a grating or a crossed grating and simulating the satellite radar with coherent optical radiation. The ratio of the optical wavelength to the length of the gratings periodicity will be equal to the ratio of the radar's wavelength and the dimensions of a city block.

# *MISSION*
# *of*
# *Rome Air Development Center*

RADC plans and executes research, development, test and selected acquisition programs in support of Command, Control, Communications and Intelligence ($C^3I$) activities. Technical and engineering support within areas of competence is provided to ESD Program Offices (POs) and other ESD elements to perform effective acquisition of $C^3I$ systems. The areas of technical competence include communications, command and control, battle management, information processing, surveillance sensors, intelligence data collection and handling, solid state sciences, electromagnetics, and propagation, and electronic, maintainability, and compatibility.

END

11-86

DTIC